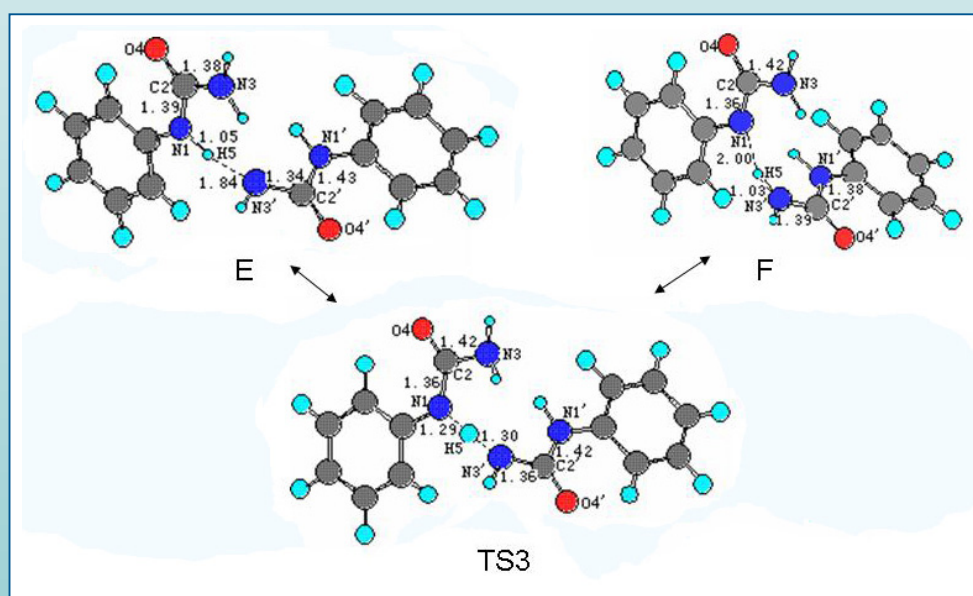


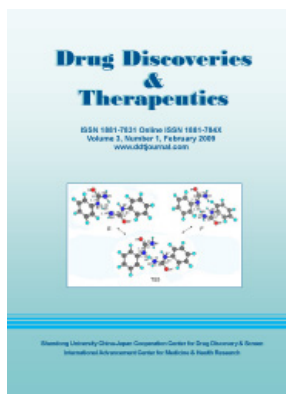
Drug Discoveries & Therapeutics

ISSN 1881-7831 Online ISSN 1881-784X
Volume 3, Number 1, February 2009
www.ddtjournal.com



Shandong University China-Japan Cooperation Center for Drug Discovery & Screen
International Advancement Center for Medicine & Health Research

Drug Discoveries & Therapeutics



Editor-in-Chief:

Kazuhisa SEKIMIZU
(The University of Tokyo, Tokyo, Japan)

Associate Editor:

Norihiro KOKUDO
(The University of Tokyo, Tokyo, Japan)

Drug Discoveries & Therapeutics is a peer-reviewed international journal published bimonthly by *Shandong University China-Japan Cooperation Center for Drug Discovery & Screen (SDU-DDSC)* and *International Advancement Center for Medicine & Health Research Co., Ltd. (IACMHR Co., Ltd.)*.

Drug Discoveries & Therapeutics mainly publishes articles related to basic and clinical pharmaceutical research such as pharmaceutical and therapeutical chemistry, pharmacology, pharmacy, pharmacokinetics, industrial pharmacy, pharmaceutical manufacturing, pharmaceutical technology, drug delivery, toxicology, and traditional herb medicine. Studies on drug-related fields such as biology, biochemistry, physiology, microbiology, and immunology are also within the scope of this journal.

Subject Coverage: Basic and clinical pharmaceutical research including Pharmaceutical and therapeutical chemistry, Pharmacology, Pharmacy, Pharmacokinetics, Industrial pharmacy, Pharmaceutical manufacturing, Pharmaceutical technology, Drug delivery, Toxicology, and Traditional herb medicine.

Language: English

Issues/Year: 6

Published by: IACMHR and SDU-DDSC

ISSN: 1881-7831 (Online ISSN 1881-784X)

Editorial and Head Office

Wei TANG, MD PhD
Secretary-in-General

TSUIN-IKIZAKA 410,
2-17-5 Hongo, Bunkyo-ku,
Tokyo 113-0033, Japan
Tel: 03-5840-9697

Fax: 03-5840-9698

E-mail: office@ddtjournal.com

URL: www.ddtjournal.com



Drug Discoveries & Therapeutics

Editorial Board

Editor-in-Chief:

Kazuhisa SEKIMIZU (*The University of Tokyo, Tokyo, Japan*)

Associate Editor:

Norihiro KOKUDO (*The University of Tokyo, Tokyo, Japan*)

Secretary-in-General:

Wei TANG (*The University of Tokyo, Tokyo, Japan*)

Office Manager:

Munehiro NAKATA (*Tokai University, Kanagawa, Japan*)

Web Editor:

Yu CHEN (*The University of Tokyo, Tokyo, Japan*)

English Editor:

Curtis BENTLEY (*Roswell, GA, USA*)

China Office:

Wenfang XU (*Shandong University, Shandong, China*)

Editors:

Yoshihiro ARAKAWA (*Tokyo, Japan*)
Santad CHANPRAPAPH (*Bangkok, Thailand*)
Fen-Er CHEN (*Shanghai, China*)
Zilin CHEN (*Wuhan, China*)
Guanhua DU (*Beijing, China*)
Chandradhar DWIVEDI (*Brookings, SD, USA*)
Mohamed F. EL-MILIGI (*Cairo, Egypt*)
Harald HAMACHER (*Tuebingen, Germany*)
Hiroshi HAMAMOTO (*Tokyo, Japan*)
Xiao-Jiang HAO (*Kunming, China*)
Langchong HE (*Xi'an, China*)
David A. HORNE (*Duarte, CA, USA*)
Yongzhou HU (*Hangzhou, China*)
Wei HUANG (*Shanghai, China*)
Yu HUANG (*Hong Kong, China*)
Hans E. JUNGINGER (*Phitsanulok, Thailand*)
Toshiaki KATADA (*Tokyo, Japan*)
Ibrahim S. KHATTAB (*Safat, Kuwait*)
Hiromichi KIMURA (*Tokyo, Japan*)
Shiroh KISHIOKA (*Wakayama, Japan*)
Kam Ming KO (*Hong Kong, China*)
Nobuyuki KOBAYASHI (*Nagasaki, Japan*)
Toshiro KONISHI (*Tokyo, Japan*)
Masahiro KUROYANAGI (*Hiroshima, Japan*)
Chun Guang LI (*Victoria, Australia*)
Hongmin LIU (*Zhengzhou, China*)
Ji-Kai LIU (*Kunming, China*)

Hongxiang LOU (*Jinan, China*)
Ken-ichi MAFUNE (*Tokyo, Japan*)
Norio MATSUKI (*Tokyo, Japan*)
Tohru MIZUSHIMA (*Kumamoto, Japan*)
Abdulla M. MOLOKHIA (*Alexandria, Egypt*)
Masahiro MURAKAMI (*Osaka, Japan*)
Yoshinobu NAKANISHI (*Ishikawa, Japan*)
Yutaka ORIHARA (*Tokyo, Japan*)
Xiao-Ming OU (*Jackson, MS, USA*)
Wei-San PAN (*Shenyang, China*)
Shafiqur RAHMAN (*Brookings, SD, USA*)
Adel SAKR (*Cincinnati, OH, USA*)
Abdel Aziz M. SALEH (*Cairo, Egypt*)
Tomofumi SANTA (*Tokyo, Japan*)
Yasufumi SAWADA (*Tokyo, Japan*)
Brahma N. SINGH (*Commack, NY, USA*)
Hongbin SUN (*Nanjing, China*)
Benny K. H. TAN (*Singapore, Singapore*)
Ren-Xiang TAN (*Nanjing, China*)
Murat TURKOGLU (*Istanbul, Turkey*)
Stephen G. WARD (*Bath, UK*)
Takako YOKOZAWA (*Toyama, Japan*)
Liangren ZHANG (*Beijing, China*)
Jian-Ping ZUO (*Shanghai, China*)

(as of February 25, 2009)

News

- 1** **China makes an impressive breakthrough in avian influenza virus research — Discovering the "heart" of avian influenza virus.**

Yonggang Li, Jifeng Wu, Xun Li

Brief Reports

- 2 - 5** **Establishment of a new cell line for high-throughput evaluation of chemokine CCR5 receptor antagonists.**

Lili Ji, Yuchen Sheng, Li Chen, Zhengtao Wang

- 6 - 9** **Formulation and evaluation of *in situ* gelling thermoreversible mucoadhesive gel of fluconazole.**

Indrajeet D. Gonjari, Avinash H. Hosmani, Amrit B. Karmarkar, Appasaheb S. Godage, Sharad B. Kadam, Pandurang N. Dhabale

Original Articles

- 10 - 12** **Computational study of the proton transfer of phenyl urea.**

Xiao Hu, Weiren Xu, Runling Wang, Xianchao Cheng, Lida Tang

- 13 - 17** **Liposomal oxytetracycline and doxycycline: studies on enhancement of encapsulation efficiency.**

Marianna Budai, Patricia Chapela, Livia Budai, Melinda E. Wales, Ilona Petrikovics, Andreas Zimmer, Pal Gróf, Imre Klebovich, Maria Szilasi

CONTENTS

(Continued)

- 18 - 26** **Study of the analgesic, anti-inflammatory, and gastric effects of gabapentin.**

Omar M. E. Abdel-Salam, Amany A. Sleem

- 27 - 36** **Enhancement of the dissolution profile of Tenoxicam by a solid dispersion technique and its analytical evaluation using HPLC.**

Manal K. Darwish, Manal M. Foad

Guide for Authors

Copyright

News

China makes an impressive breakthrough in avian influenza virus research — Discovering the "heart" of avian influenza virus

Yonggang Li¹, Jifeng Wu², Xun Li^{1,*}

Keywords: Avian influenza virus, H5N1, Polymerase, Endonuclease, PA protein

The successive appearance of strains of epizootic avian influenza A virus with the subtype H5N1 in China has attracted considerable concern from the public and Chinese authorities. According to the latest WHO estimates as of February 2, 2009, the number of H5N1 virus deaths in China totaled 25, second only to Indonesia and Viet Nam (http://www.who.int/csr/disease/avian_influenza/country/cases_table_2009_02_02/en/index.html).

The H5N1 virus is highly contagious among birds and is fatal when transmitted to humans, though the means by which this occurs is still unknown. Owing to the possible variation of the H5N1 prototype virus, together with the fact that it has the propensity to exchange genes with influenza viruses from other species, humans have no natural immunity to the virus. Despite years of efforts, the exact pathogenesis of H5N1 transmission to humans is still not completely clear, nor is potential human-to-human transmission as could lead to an epidemic or even worldwide pandemic (*Enserink M. Science. 2009; 323:324*). Unfortunately, current antiviral treatment and therapeutic measures cannot effectively overcome this virulent virus that causes highly pathogenic avian influenza (HPAI).

Researchers from around the world are working to study the virology of influenza viruses, including their methods of infiltration, replication, and transcription, to elucidate the mechanisms of unremitting viral infection in terms of aspects such as the virus, host, and environment. These researchers are also working to identify potential molecular targets related to H5N1 for anti-influenza drug intervention.

A recent H5N1-related study from China provides encouraging information. According to the People's Daily (*Renmin Ribao*), a newspaper out of Beijing, professor Liu Yingfang, academician Rao Zihe, and fellow researchers from more than 6 research centers, including the Institute of Biophysics Chinese Academy of Sciences, Nankai University, and Tsinghua University, have achieved exciting results in providing a detailed understanding of the mechanisms of action of the RNA polymerase PA subunit, the "heart" of the avian influenza virus, at the atomic level. They hope to provide clues to potential avian influenza therapy targets and a new platform for new

drug discovery (http://202.123.110.5/jrzg/2009-02/06/content_1222973.htm, available as of February 6, 2009).

According to Liu *et al.*, influenza viruses are enveloped, negatively stranded RNA viruses with a segmented genome (consisting of 8 RNA segments) that can encode 11 kinds of viral proteins. Among these proteins, the complex of influenza polymerase, consisting of PB1, PB2, and PA subunits, is regarded to be what gives life to influenza viruses because of its essential catalytic role in viral RNA replication and mRNA transcription in the nucleus of infected cells. Notwithstanding earlier virology studies on the influenza virus that elucidated the functions of PB1 and PB2, the exact function of PA is still not completely clear.

The group resolved the crystal structure of the carboxyl-terminus of PA in complex with the amino-terminus of PB1 peptides for the first time. This structure mode provides details for the interactions of PA and PB1, as well as the binding sites of PA and RNA. Results of the research, entitled the "Crystal structure of the polymerase PA(c)-CPB1(N) complex from an avian influenza H5N1 virus," were published in the August 28th issue of the respected international scientific journal *Nature* (*He X, Zhou J, Bartlam M, et al. Nature. 2008; 454:1123-1126*).

Further efforts by the group served to indicate the fine three-dimensional structure of the N-terminal of PA protein. They revealed that the PA subunit holds an endonuclease active site and that it, rather than the PB1 subunit as was previously, plays a critical role in the endonuclease activity of influenza virus polymerase. In addition, PA's characteristics of being highly conserved and having little mutations make it an attractive target for anti-influenza therapeutics. Specifically, endonuclease can block the mRNA of host cells cached by the complex of polymerase, resulting in mRNA transcription.

Results of the group's most recent research have been published in a recent February 4th issue of *Nature* (*Yuan P, Bartlam M, Lou Z, et al. Nature. 2009; Epub ahead of print*).

¹ School of Pharmaceutical Sciences, Shandong University, Ji'nan, China; ² Ji'nan Public Security Bureau, Ji'nan, China; *e-mail: tjulx2004@sdu.edu.cn

Brief Report

Establishment of a new cell line for high-throughput evaluation of chemokine CCR5 receptor antagonists

Lili Ji¹, Yuchen Sheng², Li Chen^{3,*}, Zhengtao Wang^{1,*}

¹ Key Laboratory of Standardization of Chinese Medicines of Ministry of Education, Shanghai Key Laboratory of Complex Prescription, Institute of Chinese Materia Medica, Shanghai University of Traditional Chinese Medicine, Shanghai, China;

² The Department of Pharmacology, Shanghai Institute of Pharmaceutical Industry, Shanghai, China;

³ Shanghai Target Drug Pharmaceutical Co.,Ltd., Shanghai, China.

ABSTRACT: Chemokine receptors belong to a superfamily of proteins that signal through coupled heterotrimeric G proteins. Chemokine receptor CCR5 is the major co-receptor essential for HIV entry into host cells, and now chemokine CCR5 receptor has become an important target in searching for anti-HIV drugs. Here, we describe the establishment of a human embryonic kidney (HEK) 293/CCR5-HA cell line stably expressing CCR5 receptor with influenza hemagglutinin (HA) tag at the N termini on the membrane surface of HEK293 cells. Plasmid pcDNA3.0-CCR5-HA was transfected into HEK293 cells, and monoclonal HEK293 cell lines expressing CCR5 receptor were generated under G418 selection. The expression of functional CCR5 receptor was tested by GTP γ S assay, and the results showed about 5 monoclonal HEK293 cell lines expressed functional CCR5 receptor, and of which No.7 monoclonal cell line is the best. The FACS analysis results further confirmed that CCR5 receptor was positive in 96.89% of No.7 monoclonal HEK293/CCR5-HA cell line. Further results showed that RANTES significantly stimulated GTP γ S binding in the dose-dependent manner, and CCR5 antagonist Sch-351125 inhibited RANTES-stimulated GTP γ S binding in the dose-dependent manner in No.7 monoclonal HEK293/CCR5-HA cell line. Our results suggest that the established HEK293/CCR5-HA cell line is suitable for high-

throughput screening and is feasible to identify CCR5 receptor antagonists.

Keywords: Chemokine, HEK293 cell, CCR5 receptor, Drug screening

1. Introduction

The incidence of acquired immune deficiency syndrome (AIDS) continues to increase in the world, and about 60 million people are estimated to have AIDS. In China, there are nearly 1 million people infected with human immunodeficiency virus (HIV), and this disease has been spreading aggressively ever since. An asymptomatic period precedes AIDS in which the immune system becomes progressively compromised and unable to fight opportunistic infections and certain cancers (1). The primary cell surface receptor for HIV infection is the CD4 glycoprotein, but only CD4 is not sufficient for the infection of HIV. It is now clearly established that chemokine receptors can act in concert with CD4 to enable the entry of HIV and simian immunodeficiency virus (SIV) into target cells (2-5).

Chemokines, a family of structurally related low molecular mass cytokines, are crucial to the development of lymphoid tissues and the migration of leukocytes (6). Chemokines are distinguished based on the relative position of conserved residues into four subfamilies, designated CC, CXC, C and CX3C chemokines, and chemokines exert their biological effects by binding to chemokine receptors, which belong to the seven-transmembrane G protein coupled receptor family (7).

Chemokine CCR5 receptor has recently sparked substantial interests because of its role as the co-receptor for the infection of M-tropic HIV strains (8). HIV binds to cellular membrane CD4 through

**To whom correspondence should be addressed:*

Dr. Zhengtao Wang, Key Laboratory of Standardization of Chinese Medicines of Ministry of Education, Shanghai Key Laboratory of Complex Prescription, Institute of Chinese Materia Medica, Shanghai University of Traditional Chinese Medicine, 1200 Cai Lun Road, Shanghai 201203, China;
e-mail: wangzht@hotmail.com

Dr. Li Chen, Shanghai Target Drug Pharmaceutical Co.,Ltd., Shanghai 200233, China;
e-mail: chenli8888@hotmail.com

its envelope protein gp120. This binding induces a conformational change in gp120, and then exposes the binding sites of CCR5 receptor. This process leads to the formation of a hairpin configuration with the conformational change of another HIV protein gp41, and subsequently leads to the membrane fusion (9-11). One of the approaches to the blockade of this process is through interference with the binding to CCR5 receptor, therefore, its ligands such as regulated on activation normal T-cell expressed and secreted (RANTES), macrophage inflammatory protein (MIP)-1 α , and MIP-1 β are able to block infection of M-tropic HIV strains (12). Several NH₂-terminal modifications of RANTES have also been described to block the infection by HIV-1 such as Met-RANTES, aminooxypentane (AOP)-RANTES, *etc* (13,14). Recently the small molecule CCR5 receptor antagonists have been proved to be useful in blockade of the infection of HIV-1. There are many companies and institutes apply themselves to developing and searching the CCR5 receptor antagonists, and they get some progress in this field such as TAK-779 and its derivatives, WO200066551 and its derivatives, a serial of Sch-C derivatives, *etc* (15-17). Therefore, CCR5 receptor antagonists, the next therapeutic class for treatment of HIV infection (18), have the potential to significantly alter the landscape of HIV treatment by providing a new class of drug that targets a host cellular receptor rather than a viral enzyme.

The present study describes the establishment of a stable HEK293/CCR5-HA cell line, which would be an ideal system for high-throughput screening of CCR5 receptor antagonist.

2. Materials and Methods

2.1. Cells, chemicals, and plasmids

HEK293 cells were obtained from the American Type Culture Collection (ATCC) and maintained in MEM supplemented with 10% fetal bovine serum (FBS). Recombinant human RANTES was from BD Biosciences Pharmingen, San Jose, CA, USA. Mouse mAb 12CA5 against HA epitope was obtained from Boehringer Mannheim, and FITC-conjugated goat anti-mouse IgG was from Tago, Burlingame, CA, USA. A plasmid for expressing CCR5-HA fusion protein (pcDNA3-CCR5-HA) was kindly provided by Prof. Gang Pei, Shanghai Institutes for Biological Sciences, Chinese Academy of Sciences, China (19,20). Sch-351125 was gifts from Prof. Dawei Ma, Shanghai Institute of Organic Chemistry, Chinese Academy of Sciences, China. LipofectamineTM 2000 was from Invitrogen, Carlsbad, CA, USA. [³⁵S]GTP γ S was from GE Healthcare Bio-Sciences, Piscataway, NJ, USA, and all other reagents unless indicated were from Sigma-Aldrich, St Louis, MO, USA.

2.2. Transfection and cell line establishment

HEK293 cells were transfected with the recombinant plasmid pcDNA3-CCR5-HA using LipofectamineTM 2000 according to the manufacture's instructions. Forty-eight hours post transfection transfected HEK293 cells were trypsinized and persistently cultured in MEM medium containing 0.5 mg/mL G418 for 2-3 weeks. Every resistant "cell island" was trypsinized and seeded to the 96-well plate by the limiting dilution in MEM medium containing G418 to generate signal cell clones. The G418 resistant monoclonal cell clones that grew well were selected for further analysis.

2.3. [³⁵S]GTP γ S binding assay

The assay was carried out as described (20). Cells were lysed in 5 mM Tris-HCl, pH 7.5, 5 mM EDTA, 5 mM EGTA at 4°C. The membrane pellet resulted from a 30,000 \times g centrifugation was resuspended, and aliquots containing 10 μ g protein were incubated at 30°C for 1 h in 50 mM Tris-HCl, pH 7.5, 1 mM EDTA, 5 mM MgCl₂, 100 mM NaCl, 40 μ M GDP, 0.5 nM [³⁵S]GTP γ S (1,200 Ci/mmol) in the presence or absence of the agonists in a total volume of 100 μ L. The reaction was terminated by adding cold PBS and filtered through GF/C filters, which were counted in a liquid scintillation spectrophotometer. Data were means of duplicate samples. Basal binding was determined in the absence of agonists, and nonspecific binding was obtained in the presence of 10 μ M GTP γ S. The percentage of stimulated [³⁵S]GTP γ S binding was calculated as $100 \times (\text{cpm}_{\text{sample}} - \text{cpm}_{\text{nonspecific}}) / (\text{cpm}_{\text{basal}} - \text{cpm}_{\text{nonspecific}})$.

2.4. Flow Cytometry

Cells were incubated with 5 μ g/mL anti-HA antibody in PBS containing 2% BSA at 4°C for 1 h. The presence of CCR5 chemokine receptors on the cell surface was detected by incubation with FITC-conjugated goat anti-mouse IgG. The cells were analyzed on a FACSCalibur flow cytometer. Basal cell fluorescence intensity was determined with cells stained with the secondary antibody alone.

2.5. Statistical analysis

Data were presented as mean \pm standard deviation and analyzed by the Student's *t* test using SigmaPlot 8.0. *P* < 0.05 was considered statistically significant.

3. Results and Discussion

3.1. Establishment of stable cell lines expressing CCR5-HA fusion protein

The application of stable and reliable *in vitro* cell model

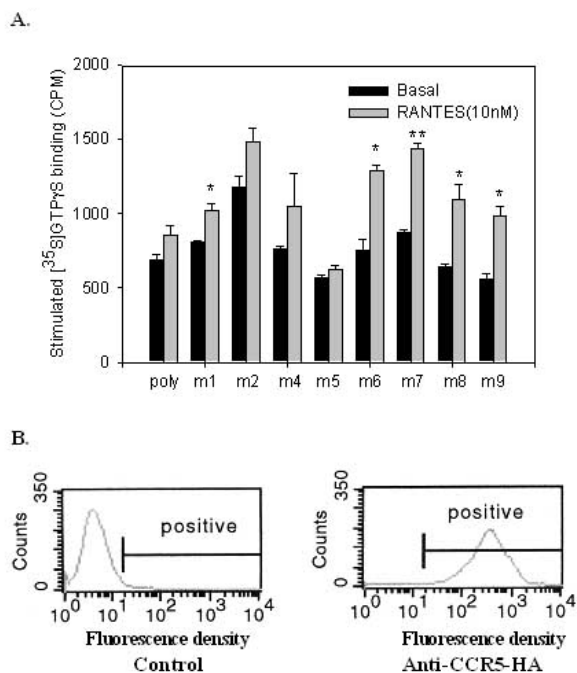


Figure 1. Establishment of the monoclonal HEK293/CCR5-HA cell line. (A) RANTES (10 nM) stimulated GTP γ S binding in the non-selected polyclonal (poly) and selected monoclonal cell lines (m1, m2, m4, m5, m6, m7, m8, m9). Data were mean \pm SD performed in duplicate. * $p < 0.05$, ** $p < 0.01$ compared with absence of RANTES. (B) FACS analysis of the expression of CCR5-HA on the membrane surface of No.7 monoclonal cell line. Cells were incubated with anti-HA antibody first, and then stained with FITC-conjugated secondary antibody and detected with a FACS scan analyzer.

is a prerequisite for the successful start of screening the CCR5 receptor antagonists. Since CCR5 receptor has no specific ligand, and since the ligands for CCR5 such as RANTES, MIP-1 α , and MIP-1 β are also the ligands for CCR1, CCR3, *etc.*, the establishment of the particular CCR5 expression cell lines is of most importance. To establish cell lines stably expressing CCR5-HA fusion protein, HEK293 cells were transfected with the plasmid pcDNA3-CCR5-HA and colonies were selected in the presence of G418 sulfate and formed some visually distinct "cell islands". Independent and G418-resistant cell islands were trypsinized and cloned by limiting dilution. After selection, eight G418 resistant clones were obtained in HEK293 cells transfected with pcDNA3-CCR5-HA. The [35 S]GTP γ S binding assay has been widely applied to determine the agonist-dependent of PTX-sensitive Gi/o proteins mediated by G-protein coupled receptors (GPCRs) (21). It has been reported that CCR5 receptor functionally couples to membrane-associated inhibitory G proteins (20), therefore, in this study we use [35 S]GTP γ S binding assay to fast observe whether the selected monoclonal cell lines express the functional CCR5 receptor. As shown in Figure 1A, there were five monoclonal cell lines expressing functional CCR5 receptor, and of which No.7 is the best. We further used FACS analysis to confirm the membrane surface expression of CCR5-HA in No.7 HEK293/CCR5-HA cells. The results showed that CCR5 was

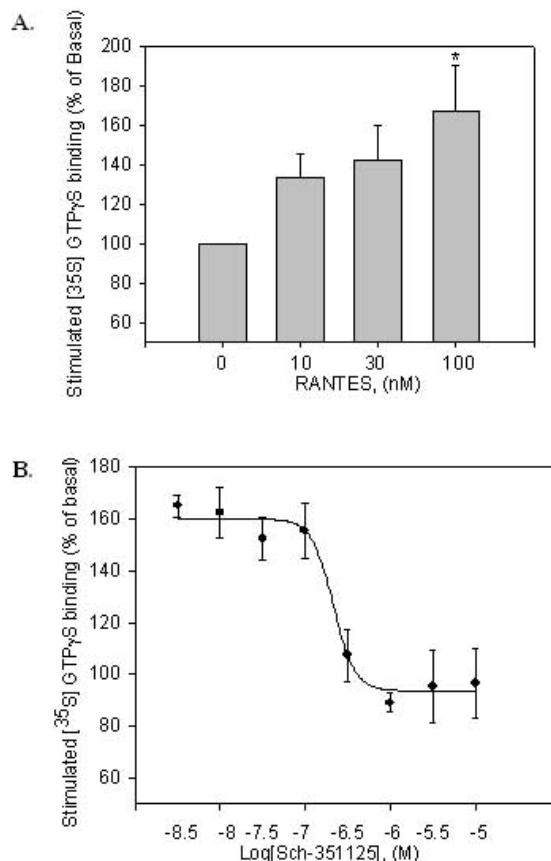


Figure 2. Functional analysis of monoclonal No.7 HEK293/CCR5-HA cells. (A) RANTES stimulated [35 S]GTP γ S binding. Data were mean \pm SD of two experiments performed in duplicate. * $p < 0.05$ compared with absence of RANTES. (B) CCR5 receptor antagonist Sch-351125 inhibited RANTES-stimulated [35 S]GTP γ S binding in No.7 HEK293/CCR5 cells. Data were mean \pm SD of two experiments performed in duplicate.

positive in 96.89% of HEK293/CCR5-HA cells (No.7), while in 2.44% of HEK293 cell (Figure 1B). All these results indicate that No.7 monoclonal cell line stably expresses chemokine CCR5 receptor on HEK293 cell membrane surface.

3.2. Functional analysis in HEK293/CCR5-HA cell line

As shown in Figure 2A, CCR5 receptor agonist RANTES stimulated GTP γ S binding in No.7 HEK293/CCR5-HA cells in the dose-dependent manner. In contrast, CCR5 receptor specific antagonist Sch-351125 inhibited RANTES-stimulated GTP γ S binding in a dose-dependent manner (Figure 2B).

In summary, this established HEK293/CCR5-HA cell line would be most valuable as a tool for high-throughput screening the antagonists of chemokine CCR5 receptor and *in vitro* evaluation of therapeutic potential in the anti-HIV therapy.

Acknowledgments

This work was partly supported by the Opening Project of Key Laboratory of Standardization

of Chinese Medicines of Ministry of Education (ZK0801).

References

1. Levy JA. HIV pathogenesis: knowledge gained after two decades of research. *Adv Dent Res.* 2006; 19:10-16.
2. Moore JP. HIV entry and tropism: the chemokine receptor connection. *AIDS.* 1997; 11:S3-S16.
3. Berger EA. Coreceptors for HIV-1 entry. *Curr Opin Immunol.* 1997; 9:551-562.
4. Dragic T, Litwin V, Allaway GP, Martin SR, Huang Y, Nagashima KA, Cayanan C, Maddon PJ, Koup RA, Moore JP, Paxton WA. HIV-1 entry into CD4+ cells is mediated by the chemokine receptor CC-CKR-5. *Nature.* 1996; 381:667-673.
5. Alkhatib G, Combadiere C, Broder CC, Feng Y, Kennedy PE, Murphy PM, Berger EA. CC CKR5: A RANTES, MIP-1 alpha, MIP-1 beta receptor as a fusion cofactor for macrophage-tropic HIV-1. *Science.* 1996; 272:1955-1958.
6. Zlotnik A, Morales J, Hedrick JA. Recent advances in chemokines and chemokine receptors. *Crit Rev Immunol.* 1999; 19:1-47.
7. Horuk R. Chemokine receptors. *Cytokine Growth Factor Rev.* 2001; 12:313-335.
8. Suresh P, Wanchu A. Chemokines and chemokine receptors in HIV infection: role in pathogenesis and therapeutics. *J Postgrad Med.* 2006; 52:210-217.
9. Kwong PD, Wyatt R, Robinson J, Sweet RW, Sodroski J, Hendrickson WA. Structure of an HIV gp120 envelope glycoprotein in complex with the CD4 receptor and a neutralizing human antibody. *Nature.* 1998; 393:648-659.
10. Rizzuto CD, Wyatt R, Hernandez-Ramos N, Sun Y, Kwong PD, Hendrickson WA, Sodroski J. A conserved HIV gp120 glycoprotein structure involved in chemokine receptor binding. *Science.* 1998; 280:1949-1953.
11. Wu L, LaRosa G, Kassam N, Gordon CJ, Heath H, Ruffing N, Chen H, Humblis J, Samson M, Parmentier M, Moore JP. Interaction of chemokine receptor CCR5 with its ligands: multiple domains for HIV-1 gp120 binding and a single domain for chemokine binding. *J Exp Med.* 1997; 186:1373-1381.
12. Cocchi F, DeVico AL, Garzino-Demo A, Arya SK, Gallo RC, Lusso P. Identification of RANTES, MIP-1 alpha, and MIP-1 beta as the major HIV-suppressive factors produced by CD8+ T cells. *Science.* 1995; 270:1811-1815.
13. Proudfoot AEI, Power CA, Hoogewerf AJ, Montjovent MO, Borlat F, Offord RE, Wells TN. Extension of recombinant human RANTES by the retention of the initiating methionine produces a potent antagonist. *J Biol Chem.* 1996; 271:2599-2603.
14. Mack M, Luckow B, Nelson PJ, Cihak J, Simmons G, Clapham PR, Signoret N, Marsh M, Stangassinger M, Borlat F, Wells TN, Schlondorff D, Proudfoot AE. Aminooxypentane-RANTES induces CCR5 internalization but inhibits recycling: a novel inhibitory mechanism of HIV infectivity. *J Exp Med.* 1998; 187:1215-1224.
15. Kazmierski W, Bifulco N, Yang HB, Boone L, DeAnda F, Watson C, Kenakin T. Recent progress in discovery of small-molecule CCR5 chemokine receptor ligands as HIV-1 inhibitors. *Bioorg Med Chem.* 2003; 11:2663-2676.
16. Baba M, Takashima K, Miyake H, Kanzaki N, Teshima K, Wang X, Shiraishi M, Iizawa Y. TAK-652 inhibits CCR5-mediated human immunodeficiency virus type 1 infection *in vitro* and has favorable pharmacokinetics in humans. *Antimicrob Agents Chemother.* 2005; 49:4584-4591.
17. Tsamis F, Gavrilo S, Kajumo F, Seibert C, Kuhmann S, Ketas T, Trkola A, Palani A, Clader JW, Tagat JR, McCombie S, Baroudy B, Moore JP, Sakmar TP, Dragic T. Analysis of the mechanism by which the small-molecule CCR5 antagonists Sch-351125 and Sch-350581 inhibit human immunodeficiency virus type 1 entry. *J Virol.* 2003; 77:5201-5208.
18. Julg B, Goebel FD. CCR5 antagonists: a new tool in fighting HIV. *J HIV Ther.* 2005; 10:68-71.
19. Ling K, Wang P, Zhao J, Wu YL, Cheng ZJ, Wu GX, Hu W, Ma L, Pei G. Five-transmembrane domains appear sufficient for a G protein-coupled receptor: Functional five-transmembrane domain chemokine receptors. *Proc Natl Acad Sci U S A.* 1999; 96:7922-7927.
20. Zhao J, Ma L, Wu YL, Wang P, Hu W, Pei G. Chemokine receptor CCR5 functionally couples to inhibitory G proteins and undergoes desensitization. *J Cell Biochem.* 1998; 71:36-45.
21. Traynor JR, Nahouaki SR. Modulation by mu-opioid agonists of guanosine-5'-O-(3-[³⁵S]thio)triphosphate binding to membranes from human neuroblastoma SHSY5Y cells. *Mol Pharmacol.* 1995; 47:848-854.

(Received December 29, 2008; Revised January 4, 2009; Accepted January 4, 2009)

Brief Report

Formulation and evaluation of *in situ* gelling thermoreversible mucoadhesive gel of fluconazole

Indrajeet D. Gonjari^{1,*}, Avinash H. Hosmani², Amrit B. Karmarkar¹, Appasaheb S. Godage¹, Sharad B. Kadam¹, Pandurang N. Dhabale¹

¹ Government College of Pharmacy, Satara, MS, India;

² Government College of Pharmacy, Amaravati, MS, India.

ABSTRACT: The purpose of the present study was to develop ophthalmic gel formulations of fluconazole. Intraocular delivery of topically applied drugs such as fluconazole is hampered by elimination of the solution due to tear turnover, so an *in situ* gelling thermoreversible mucoadhesive gel was formulated. Thermoreversible mucoadhesive gels were prepared using the cold method along with poloxamer 407 and different mucoadhesive polymers such as hydroxy ethyl cellulose (HEC), hydroxy propyl methyl cellulose (HPMC) K4M, and polyvinyl pyrrolidone (PVP) K30. Gels were evaluated for physical parameters like appearance, gelation temperature, pH, spreadability, drug content, gel strength, bioadhesion, and *in vitro* permeation. A modified device (modified K-C diffusion cell with a sheep's eye corneal membrane as a diffusion membrane) was used for evaluation of drug permeation through a sheep's corneal membrane. The formulated gels were transparent, uniform in consistency, and had spreadability with a pH range of 6.8 to 7.3. Satisfactory bioadhesion on the sheep's corneal surface and good gel strength were also observed. Diffusion studies have shown that a matrix is the best-fit model. As the concentration of mucoadhesive agent increases, the rate of permeation decreases. The order of drug permeation through the membrane was HEC > PVP K30 > HPMC K4M. This study found that a thermoreversible polymer and mucoadhesive polymers can be effectively used to prolong residence time.

Keywords: Ophthalmic gels, Poloxamer 407, Mucoadhesive polymers, *In situ* gelling

*To whom correspondence should be addressed:

Dr. Indrajeet D. Gonjari, Department of Pharmaceutics, Government College of Pharmacy, Karad-415124, Dist. Satara, MS, India;
e-mail: indrajeetgonjari@gmail.com

1. Introduction

In the field of pharmaceutical research, ophthalmic delivery is extremely interesting and highly challenging (1,2). Topical ocular infections and especially fungal infections can be effectively treated with ocular delivery itself rather than using an oral delivery of drugs. Popular treatments such as eye drops and suspensions are available for topical administration of ophthalmically active drugs to tissues around the ocular cavity. These suffer from a drawback in that the active constituent becomes diluted in tear film as the preparation is instilled into the *cul-de-sac* and is rapidly drained away from pre-corneal cavity by constant tear flow and lacrimo-nasal drainage. As a result, only a small fraction of the dose is absorbed by ocular tissues. Hence, frequent administration and use of concentrated solutions serve to provide the desired therapeutic effect (3). Candidal endophthalmitis is a sight-threatening ocular infection that most frequently occurs as a complication of candidemia. Fluconazole is a fluorinated bis-triazole derivative that has been reported to be effective against *Candida albicans* in various experimental animal models and clinical settings (4).

Thermoreversible gels made of poloxamer 407 have *in situ* gelling behavior (5). *In situ* gels formulated using poloxamer 407 can be conveniently applied to the conjunctival sac, where they undergo transition from a sol to a gel. Prolongation of residence time due to these *in situ* gelling systems will help to deliver a drug continuously in a controlled manner to the anterior chamber of eye, eliminating the need for frequent administration of drug and thus resulting in better patient compliance and prolonged action. This will result in a dose reduction, helping to minimize local and systemic side effects (6). In the present study, mucoadhesive polymers such as hydroxy propyl methyl cellulose (HPMC) K4M, hydroxy ethyl cellulose (HEC), and polyvinyl pyrrolidone (PVP) K30 were used to prolong the residence time of the gels and may

have helped to provide an additional advantage to gels containing poloxamer 407 alone.

2. Materials and Methods

2.1. Materials

Fluconazole was donated by Glenmark Pharmaceuticals (Mumbai, India), poloxamer 407 was donated by BASF India (Mumbai, India), and HEC, HPMC K4M, and PVP K30 were supplied by Cipla (Mumbai, India). All other chemicals used were of analytical grade.

2.2. Methods

Thermoreversible mucoadhesive gels of fluconazole were prepared using the cold method (7). Accurately weighed quantities of fluconazole and mucoadhesive polymer (Table 1) were dissolved in sterile water. To these solutions the required amount of poloxamer 407 was added. Weight was adjusted with distilled water to reach a final concentration of fluconazole of 0.2% (w/w). The solution was mixed well and stored at 4°C for 12 h. All solutions were adjusted to a pH in the range of 6.8 to 7.3 with the help of 2 M NaOH. All gel formulations were evaluated for physical appearance, consistency and spreadability.

2.3. Measurement of gelation temperature

Gelation temperatures of the gels were measured according to the method described by Gilbert *et al.* (8). Two mL aliquots of the gel were transferred in a test tube sealed with a parafilm and immersed in a water bath at 4°C. The temperature of the bath was increased in increments of 1°C and left to equilibrate for 15 min at each new setting. The samples were examined for gelation, which is considered to have occurred when the meniscus would no longer move when tilted more than 90°. All measurements were performed in triplicate ($n = 3$).

2.4. Content uniformity

All prepared gel formulations were tested for content uniformity.

2.5. In vitro bioadhesion evaluations

The bioadhesive force of all of the batches was determined by the method described by Choi *et al.* (9). A sheep's corneal membrane was cut from the eye of a sheep and instantly fixed with the mucosal side outwards onto a glass vial using a rubber band. Vials with the corneal membrane were stored at 37°C for 5 min. Then, the next vial with a section of membrane was connected to a balance in an inverted position while the first vial was placed on a height adjustable pan. The gel was placed onto the corneal membrane of the first vial. Then, the height of the second vial was adjusted so that the membrane surfaces of both vials came in close contact. A ten minute contact time was chosen. Then, the weight was allowed to increase in the pan until the vials had detached. The bioadhesive force was the minimum weight required to detach two vials. The corneal membrane was replaced for each measurement ($n = 3$).

2.6. Measurement of gel strength

A sample of 50 g of gel was placed in a 100 mL graduated cylinder and gelled in a thermostat at 37°C. The apparatus for measuring gel strength as described by Choi *et al.* (9) was allowed to penetrate the gel. Gel strength, *i.e.* the viscosity of the gels at physiological temperature, was determined by the time (in seconds) taken by the apparatus to sink down 5 cm through the prepared gel. All measurements were performed in triplicate ($n = 3$).

2.7. Permeation studies across a sheep's corneal membrane

A modified device (modified K-C diffusion cell with a sheep's eye corneal membrane as a diffusion membrane) was used for evaluation of drug permeation through a sheep's corneal membrane. This membrane was tied to a specifically designed glass cylinder (open at both ends). Simulated tear fluid (NaHCO₃ 0.218 g, NaCl 0.678 g, CaCl₂•2H₂O 0.0084 g, and KCl 0.138 g in 100 mL of water) was used as the diffusion medium. The formulation to be tested was added to the donor chamber with the help of a micropipette.

Table 1. Formulation design of thermoreversible mucoadhesive gels of fluconazole

	Formulation contents (% w/w)								
	F1	F2	F3	F4	F5	F6	F7	F8	F9
Fluconazole	0.2	0.2	0.2	0.2	0.2	0.2	0.2	0.2	0.2
Poloxamer 407	18	18	18	18	18	18	18	18	18
HEC	0.5	1	1.5						
HPMC K4M				0.5	1	1.5			
PVP							0.5	1	1.5
2M NaOH	q.s.	q.s.	q.s.	q.s.	q.s.	q.s.	q.s.	q.s.	q.s.
Sterile water	q.s.	q.s.	q.s.	q.s.	q.s.	q.s.	q.s.	q.s.	q.s.

Table 2. Results of various evaluation parameters

Formulation	Gelation temperature (°C)	Content uniformity (%)	Bioadhesion potential (dynes/cm ²)	Gel strength (sec)
F1	36.66 ± 0.32	100.5 ± 0.15	3,438.00 ± 6.04	105.33 ± 0.57
F2	35.16 ± 0.40	100.2 ± 0.05	4,039.5 ± 11.78	111.66 ± 0.57
F3	33.93 ± 0.65	99.90 ± 0.20	4,288.8 ± 16.18	117.66 ± 1.52
F4	35.36 ± 0.55	99.8 ± 0.15	4,464.06 ± 8.28	123.33 ± 0.55
F5	33.10 ± 0.55	100.2 ± 0.10	5,055.66 ± 10.1	129.3 ± 1.52
F6	31.86 ± 0.45	100.16 ± 0.05	4,953.03 ± 20.99	131.66 ± 0.57
F7	31.56 ± 0.20	101.1 ± 0.08	5,134.41 ± 11.22	135.33 ± 0.57
F8	29.10 ± 0.69	100.2 ± 0.06	5,376.41 ± 6.69	137.33 ± 0.57
F9	27.63 ± 0.30	100.1 ± 0.18	5,423.07 ± 9.44	137.66 ± 1.52

Table 3. Permeation kinetics of various formulation batches

Formulation	Zero order kinetics (R^2)	First order kinetics (R^2)	Matrix model (R^2)	Peppas model (R^2)	Hixon-Crowell model (R^2)	Korsmeyer-Peppas kinetics release exponent (n)
F1	0.8293	0.8310	0.9902	0.9806	0.8304	0.4361
F2	0.7909	0.7929	0.9840	0.9801	0.7923	0.3890
F3	0.8141	0.8159	0.9866	0.9734	0.8153	0.4292
F4	0.8068	0.8087	0.9864	0.9775	0.8081	0.4158
F5	0.7828	0.7847	0.9789	0.9593	0.7841	0.4129
F6	0.7929	0.7998	0.9832	0.9692	0.7992	0.4229
F7	0.8489	0.8504	0.9887	0.9674	0.8499	0.5003
F8	0.8607	0.8623	0.9908	0.9717	0.8618	0.4820
F9	0.8459	0.8474	0.9778	0.9342	0.8469	0.5117

The donor surface of the membrane was constantly in contact with the simulated tear fluid. A temperature of $37 \pm 0.5^\circ\text{C}$ was maintained throughout the study. A magnetic stirrer to the cell provided continuous agitation. At regular time intervals, 1 mL of sample was withdrawn and replaced by fresh simulated tear fluid in order to maintain sinking conditions. The samples were appropriately diluted and the absorbance was measured at 261.5 nm using a Shimadzu 1700UV-VIS spectrophotometer.

3. Results and Discussion

The prepared ophthalmic gel formulations exhibited optimum physical properties. Gels were transparent, uniform in consistency, and had spreadability with a pH range of 6.8 to 7.3.

3.1. Measurement of gelation temperature

As the concentration of mucoadhesive polymers increased, the gelation temperature of gel decreased (Figure 1). This ability of mucoadhesive polymers to lower gelation temperature may be due to increased viscosity after dissolution of polymers. The ability of mucoadhesive polymers to lower gelation temperature could be explained by their ability to bind to the polyoxyethylene chains present in the poloxamer 407 molecules. This would promote dehydration, causing an increase in entanglement of adjacent molecules and extensively increasing intermolecular hydrogen bonding, thus leading to gelation at lower temperature (10). Increasing the concentration of any

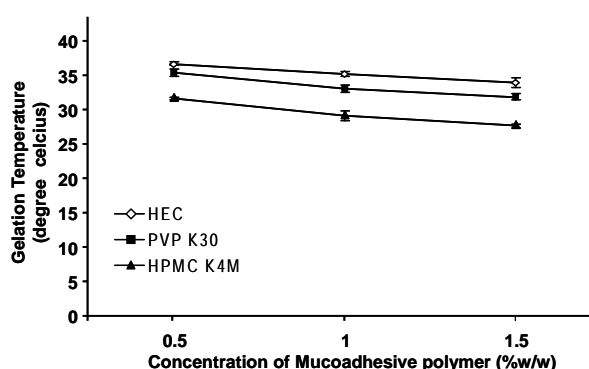


Figure 1. Effect of concentration of mucoadhesive polymer on gelation temperature.

of the mucoadhesive polymers used from 0.5 to 1.5% produced a gradual decrease in the gelation temperature of the corresponding solutions. Action to lower gelation temperature for the gels prepared using mucoadhesive polymers was, in order, HEC > PVP K30 > HPMC K4M. The results of gelation temperatures of different formulations are indicated in Table 2.

3.2. In vitro permeation studies

In vitro permeation across the sheep's corneal membrane was fit to various kinetic models of release (Figure 2). All batches indicated that a matrix model of permeation kinetics was the best-fit model. A faster release initially indicates that the drug in the solution in the space outside the gel matrix initially diffuses quickly. The release of drug within the gel is controlled by both the nature and concentration of polymer

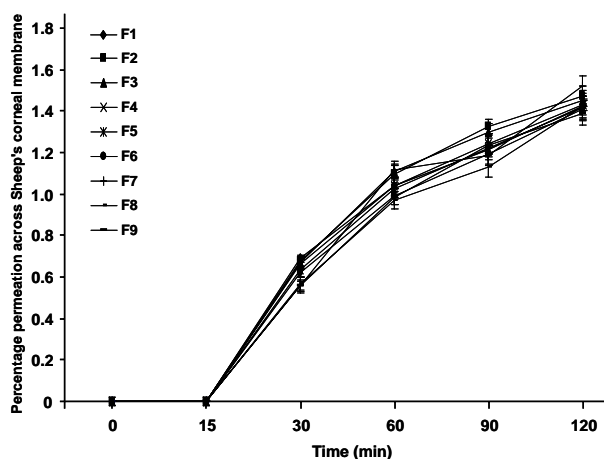


Figure 2. Permeation profile of *in situ* gelling thermoreversible gels of fluconazole.

used. Drug permeation through the cornea with a thermoreversible gel containing various mucoadhesive polymers occurred in the order of HEC > PVP K30 > HPMC K4M. 'n' values (Table 3) greater than 0.5 indicate non-Fickian release whereas those less than 0.5 indicate Fickian release.

4. Conclusion

In this study, an *in situ* gelling thermoreversible ophthalmic gel of fluconazole was developed using poloxamer 407 and various mucoadhesive polymers. These *in situ* gelling formulations were free-flowing, transparent, had uniform consistency, and had spreadability at room temperature. A satisfactory gelation temperature and bioadhesion were observed in these gels. *In vitro* permeation studies across corneal mucosa showed both Fickian and non-Fickian release. Therefore, these gels represent a viable alternative to conventional eye drops. This study demonstrated that a thermoreversible polymer and mucoadhesive

polymer can effectively be used to prolong residence time.

References

1. Ashim KM. Ophthalmic drug delivery system. Vol. 58. Marcel Dekker, New York, USA, 1993; pp. 105-110.
2. Indu P, Kaur AG, Anil KS, Deepika A. Vesicular systems in ocular drug delivery an overview. *Int J Pharm.* 2004; 269:1-14.
3. Chien YW. Ocular drug delivery and delivery systems. Chapter 6. In: *Novel Drug Delivery Systems*. Marcel Dekker, New York, USA, 1996; pp. 269-270.
4. Velpandian T, Narayanan K, Nag TC, Ravi AK, Gupta SK. Retinal toxicity of intravitreally injected plain and liposome formulation of fluconazole in rabbit eye. *Ind J Ophthalmology.* 2006; 54:237-240.
5. Karmarkar AB, Gonjari ID, Hosmani AH. Poloxamers and their applications. Online international pharmaceutical journal *Pharmainfo.net*, 2008 (<http://www.pharmainfo.net/>).
6. Edsman K, Carlfors J, Peterson R. Rheological evaluation of Poloxamer as *in situ* gel for ophthalmic use. *Eur J Pharm Sci.* 1998; 6:105-112.
7. Schmolka IR. A review of block polymer surfactants. *J Am Oil Chem Soc.* 1977; 54:110-116.
8. Gilbert JC, Richardson JL, Davies MC, Palin KJ, Hadgraft J. The effect of solutes and polymers on the gelation properties of Pluronic F127 solutions for controlled drug delivery. *J Control Release.* 1987; 5:113-118.
9. Choi HG, Jung JH, Ryu JM, Yoon SJ, Oh YK, Kim CK. Development of *in situ*-gelling and mucoadhesive acetaminophen liquid suppository. *Int J Pharm.* 1998; 165:33-44.
10. Puglia C, Bonina F, Trapani G, Franco M, Ricci M. Evaluation of *in vitro* percutaneous absorption of lorazepam and clonazepam from hydro-alcoholic gel formulations. *Int J Pharm.* 2001; 228:79-87.

(Received January 29, 2009; Accepted February 11, 2009)

Original Article

Computational study of the proton transfer of phenyl urea

Xiao Hu¹, Weiren Xu², Runling Wang^{1,*}, Xianchao Cheng¹, Lida Tang³¹ School of Pharmacy, Tianjin Medical University, Tianjin, China;² Tianjin Key Laboratory of Molecular Design and Drug Discovery, Tianjin Institute of Pharmaceutical Research, Tianjin, China;³ Tianjin Key Laboratory of Pharmacokinetics and Pharmacodynamics, Tianjin Institute of Pharmaceutical Research, Tianjin, China.

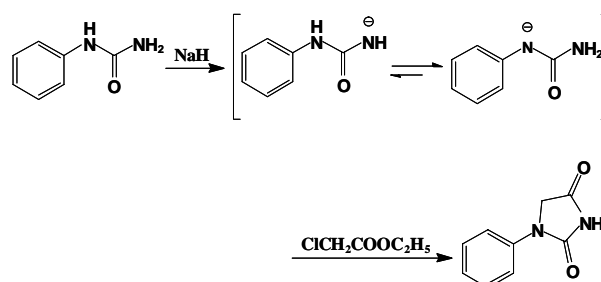
ABSTRACT: The proton transfer between two nitrogen atoms (N1 and N3) in a molecule of phenyl urea is an important process in the synthesis of 1-phenylimidazolidine-2,4-dione. Three pathways of the proton transfer have been investigated using Density Functional Theory (DFT). With negative N1 phenyl urea, the transformed double bond of N1-C2 connects N1, C2, and N3 into a benzene conjugate system, making the structure more stable than negative N3 phenyl urea. Intermolecular proton transfer was found to be the primary manner of protein transfer at 300 K. Both negative N1 and negative N3 exist and the former is primal. The proton transfer is very fast, and the diluted solution may slow down the rate but produce much more negative N1 as well.

Keywords: Proton transfer, Synthesis, DFT, B3LYP, Phenyl urea

1. Introduction

1-Phenylimidazolidine-2,4-dione is an important immediate used in the medical and chemical industries (1). It can be synthesized through phenyl urea and ethyl chloroacetate with the deprotonation of NaH. The proton transfer of phenyl urea is an important process in this synthesis. As this proton transfer can form two kinds of negative N phenyl urea as depicted in Scheme 1, there are always several co-products when this transfer actually occurs.

Based on actual performance, a hydrogen can be released during the reaction after the formation of the negative phenyl urea. There are three proton transfers involving negative phenyl urea: proton translocation between the hydrogen and phenyl urea anion, intramolecular proton translocation, and intermolecular



Scheme 1. Synthesis of 1-phenylimidazolidine-2,4-dione.

proton translocation. This study sought to investigate the theoretical mechanisms of these proton transfers using Density Functional Theory and to provide theoretical suggestions for more effective synthesis.

2. Materials and Methods

Computations were carried out using the Gaussian 98 program (2). The initial structures of reagents, products, and transition states were optimized using density functional theory (DFT) at the B3LYP/6-31G* level (3-5). To confirm the transition states, pathways were identified by intrinsic reaction coordinate (IRC) calculation (6). The frequencies of these optimized structures were also calculated to obtain the enthalpy energy and the Gibbs' free energies (G). All data and structures mentioned below are related to the same level.

3. Results and Discussion

Three possible proton transfers relating to the negative nitrogen ion are shown in Figures 1-3. The relative atomic charge distributions of all states are calculated and given in Table 1. Table 2 lists the parameters for the three reaction pathways. Figure 4 shows the relative energy changes.

Following NaH deprotonation, one H₂ molecule must be produced. The proton transfer between H₂ and a phenyl urea anion is shown in Figure 1. The computed N1-C2 distances are 1.46, 1.41, and 1.35 Å in state A, TS1, and state B, respectively, and the bond lengths of C2-N3 are 1.32, 1.36, and 1.43 Å in state A,

*To whom correspondence should be addressed:
Dr. Wang Runling, School of Pharmacy, Tianjin Medical University, Tianjin 300070, China;
e-mail: wangrunling@tjmu.edu.cn

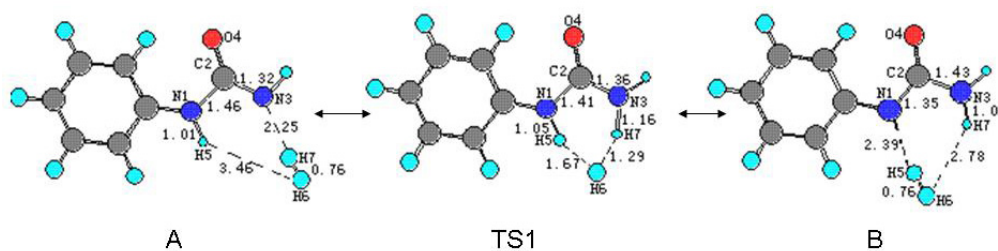


Figure 1. Proton transfer between H₂ and a phenyl urea anion and the B3LYP/6-31G* optimized structures of A, TS1, and B. Distances in Å.

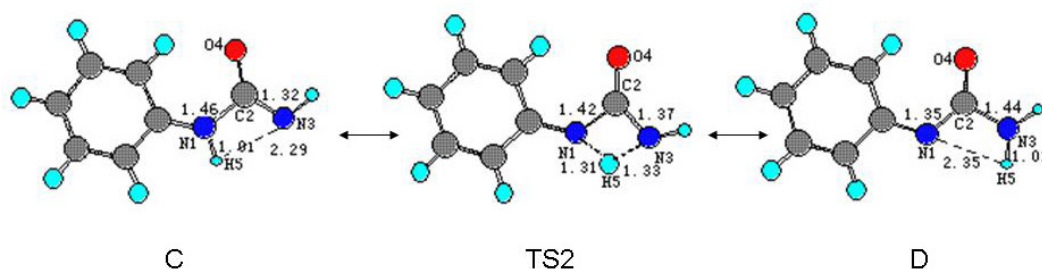


Figure 2. Intramolecular proton transfer and the B3LYP/6-31G* optimized structures of C, TS2, and D. Distances are in Å.

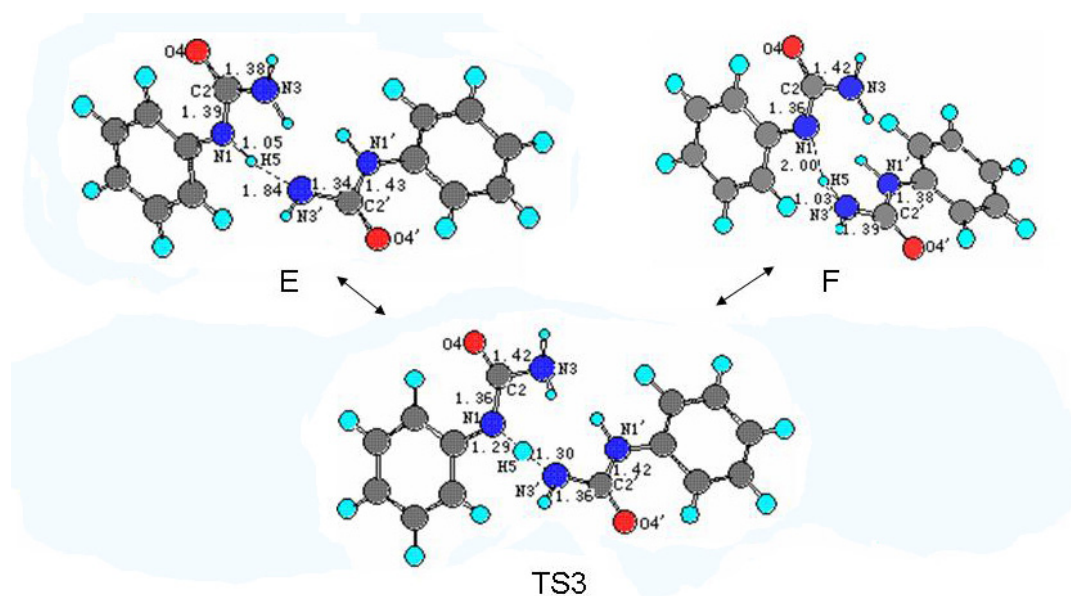


Figure 3. Intermolecular proton transfer and the B3LYP/6-31G* optimized structures of E, TS3, and F. Distances are in Å.

Table 1. The relative atomic charge distributions of all states calculated at B3LYP/6-31G*

	A	TS1	B	C	TS2	D	E	TS3	F
N1	-0.774	-0.508	-0.535	-0.723	-0.565	-0.706	-0.300	-1.007	-0.498
C2	0.876	0.715	0.694	0.843	0.722	0.748	0.723	0.957	0.767
N3	-0.969	-0.798	-0.861	-1.066	-0.840	-0.848	-0.775	-0.935	-0.888
O4	-0.697	-0.597	-0.562	-0.690	-0.614	-0.605	-0.595	-0.645	-0.642
N1'							-0.687	-0.649	-0.272
C2'							0.823	0.835	0.611
N3'							-0.720	-0.949	-0.641
O4'							-0.681	-0.634	-0.579

Charges in e.

Table 2. Energy changes and reaction equilibrium constants of three proton transfer pathways

Pathway	$\Delta H_{\text{reagent-product}}$ (kJ/mol)	$\Delta G_{\text{reagent-product}}$ (kJ/mol)	$\Delta G_{\text{forward}}$ (kJ/mol)	K_{forward}^a (1/S)	$\Delta G_{\text{reverse}}$ (kJ/mol)	K_{reverse}^a (1/S)
A-B	-18.84	-15.94	95.60	1.11E - 04	79.66	6.86E - 02
C-D	-23.41	-22.34	140.61	1.44E - 12	118.27	1.18E - 08
E-F	-3.57	-1.75	13.79	2.38E + 10	12.04	4.83E + 10

^a $K = 6.2125 \times 10^{12} \cdot \exp(-\Delta G^{\ddagger} / 1000 / (8.314 \times 298.15))$.

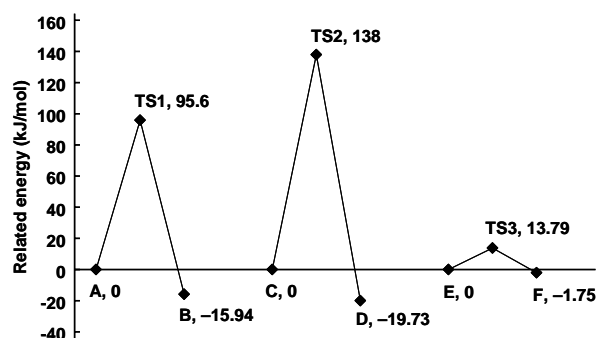


Figure 4. The relative energy changes of all pathways according to the optimized structures calculated at B3LYP/6-31G*.

TS1, and state B, respectively. Since the bond of N1-C2 is converted from a single bond to a double bond, the conjugate effect between urea and the benzene ring is enhanced. As the result, the charge values of N1, C2, and N3 decrease while the charge value for the benzene ring increases (Table 1). The charge distribution of the whole molecule becomes more uniform. Inversely, the double bond of C2-N3 becomes a single bond. In transition state 1, a planar hexatomic ring consisting of N1, C2, N3, H5, H6, and H7 connects to the conjugate area of the benzene ring.

With H5 transferred from N1 to N3, as displayed in Figure 2, intramolecular proton transfer is complete. Except for hydrogen, state C is similar to state A in terms of structure and charge distribution, while D is similar to B. In transition state 2 (TS2), N1, C2, N3, and H5 make up of a planar four-membered ring. For the bond of N1-C2 to become a double bond, the four-membered ring is conjugated with the benzene ring.

Intermolecular proton transfer is displayed in Figure 3 with the proton H5 shifting between N1 and N3'. The structures of negative molecules in states E and F are similar to those in states C and D, respectively. One can consider state C to transform into state D with the help of a phenyl urea molecule, which serves as an H-bond donor. In transition state 3 (TS3), two molecules are in different planes. N1 and N3' share H5 in a straight line. The distances of N1-H5, and N3'-H5 are 1.29 and 1.30 Å, respectively.

As shown in Table 1, the intermolecular H-bond can change the electric charge distribution. In state E, the related atoms of the negative molecule (N1', C2', N3', and O4') have lower charges than those in states A and C. This is similar to state F, where the related atomic charges of the negative molecule (N1, C2, N3, and O4) are lower than those in states B and D. Thus, the conjugate effect is stronger and the charge distribution becomes more uniform. There is a substantial correlative change between the charge and bond. An

interesting finding with regard to TS3 is that all of the atomic charges have obviously risen in comparison to TS1 and TS2. This suggests that the dipolarity of the whole system is enhanced and that conjugation weakens in TS3.

According to Table 2, all proton transfers are exothermic reactions. The pathway E to F has a lower energy barrier (Figure 4) of 13.79 kJ/mol and is the main proton transfer at 300 K. The equilibrium proportion of structures E and F is 1:2. Thus, both the negative N1 and negative N3 structures can exist together. Theoretically, there are two negative phenyl urea formed, N1 (as expected) and N3. The rate of the transfer between N1 and N3 is very fast. As indicated by the current study, the concentrated solution facilitates formation of an intermolecular complex to allow proton transfer between molecules and it also allows the formation of negative N3 phenyl urea. A diluted solution was chosen to keep the molecule simple. Although this slows down the reaction rate, a much more stable negative N1 phenyl urea is produced in the solution.

Acknowledgements

The authors are grateful for financial support from the Ministry of Science and Technology of the People's Republic of China (No. 2007BA141B01), Tianjin Municipal Science and Technology Commission, and Shanghai Supercomputer Center.

References

1. Niwata S, Fukami H, Sumida M, *et al.* Substituted 3-(phenylsulfonyl)-1-phenylimidazolidine-2,4-dione derivatives as novel nonpeptide inhibitors of human heart chymase. *J Med Chem.* 1997; 40:2156-2163.
2. Frisch MJ, Trucks GW, Schlegel HB, *et al.* Gaussian 98, Revision A.9; Gaussian, Inc., Pittsburgh, PA, USA, 1998.
3. Becke AD. Density-functional thermochemistry. III. The role of exact exchange. *J Chem Phys.* 1993; 98:5648.
4. Lee C, Yang W, Parr RG. Development of the Colle-Salvetti correlation-energy formula into a functional of the electron density. *Phys Rev B.* 1988; 37:785-789.
5. Stephens PJ, Devlin FJ, Chabalowski CF, Frisch MJ. Ab-initio calculation of vibrational absorption and circular-dichroism spectra using density-functional force-fields. *J Phys Chem.* 1994; 98:11623-11627.
6. Gonzalez C, Schlegel HB. Reaction path following in mass-weighted internal coordinates. *J Phys Chem.* 1990; 94:5523-5527.

(Received January 23, 2009; Accepted January 30, 2009)

Original Article

Liposomal oxytetracycline and doxycycline: studies on enhancement of encapsulation efficiency

Marianna Budai^{1,2,*}, Patricia Chapela², Livia Budai³, Melinda E. Wales⁴, Ilona Petrikovics², Andreas Zimmer⁵, Pal Gróf⁶, Imre Klebovich¹, Maria Szilasi⁷

¹ Semmelweis University, Department of Pharmaceutics, Budapest, Hungary;

² Sam Houston State University, Department of Chemistry, Huntsville, TX, USA;

³ Department of Mass Spectrometry, Chemical Research Centre of the Hungarian Academy of Sciences, Budapest, Hungary;

⁴ Texas A&M University, Department of Biochemistry and Biophysics, College Station, TX, USA;

⁵ Karl-Franzens University, Department of Pharmaceutical Technology, Graz, Austria;

⁶ Semmelweis University, Institute of Biophysics and Radiation Biology, Budapest, Hungary;

⁷ University of Debrecen, Medical and Health Science Center, Department of Pulmonology, Debrecen, Hungary.

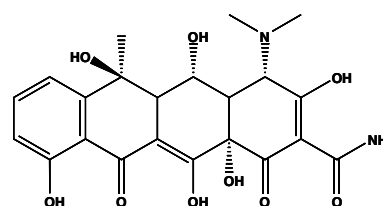
ABSTRACT: Liposomal encapsulations of oxytetracycline (OTC) and doxycycline (DC) with various lipid compositions and hydrating solutions have been studied in order to develop a new liposomal formulation to treat bacterial infections. Encapsulation efficiencies as a function of pH (pH 4.0-8.0) in ionic (phosphate buffers) and non-ionic (mannitol or glucose) hydrating solutions with various lipid compositions (lecithin or α -L-dipalmitoylphosphatidylcholine, with or without cholesterol) were determined and compared to the character of lipid vesicles. Based on our encapsulation efficiency studies and on the drug stability considerations it can be concluded that for OTC/DC encapsulation the use of non-ionic solutions is the most promising.

Keywords: Liposomal antibiotics, Oxytetracycline, Doxycycline, Encapsulation efficiency, Nano-delivery systems

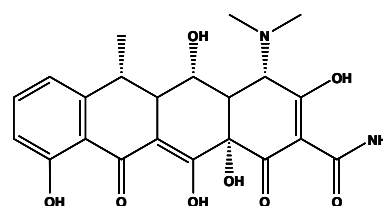
1. Introduction

Oxytetracycline (OTC) and doxycycline (DC) are bacteriostatic agents exhibiting broad spectra of activity against many different aerobic and anaerobic bacteria (Figure 1). Despite of their broad antibacterial spectra, resistance of many bacterial groups has been reported with both of them (1). Furthermore, under abnormal conditions (heat, pH, humidity), tetracyclines undergo

reversible epimerisation at positions C4 and C6 (2-5). The degradation products have very low antibiotic activity; in addition, some of them can be toxic. OTC is commonly used against external bacterial infections of the eye, such as keratoconjunctivitis, neonatal conjunctivitis, ocular rosacea or trachoma (6-10). In the ophthalmologic practice the so-called "oxytetracycline-eye-drop" is a frequently prescribed drug, prepared in pharmacies *ex tempore* with a short half life of only 3 days (11). The half-life of OTC in water was found to be 34 hours (12), thus hindering the safe use of the antibiotic preparations (13). To overcome the problems of bacterial resistance and chemical instability, liposomal formulations are being developed. The advantages of liposome entrapped drugs have been well documented (14). Liposomal carriers of encapsulated



Oxytetracycline



Doxycycline

Figure 1. Chemical structures of oxytetracycline and doxycycline.

*To whom correspondence should be addressed:

Dr. Marianna Budai, Semmelweis University, Department of Pharmaceutics, Hőgyes E. u. 7., Budapest, H-1092, Hungary; e-mail: bmariann@gyok.sote.hu

OTC or DC also offer the potential for greater penetration and prolonged release of the delivered tetracycline derivatives. In addition, lipid vesicles may provide advantages of chemical stability, similarly as observed for the reverse micelles (12). Improvement in OTC stability can be attained with reverse micellar systems. Dissolving OTC in reverse micelles, its half-life increases to 2,402 hours (12). There are no data on liposomal OTC formulations; however, encapsulation rates with some selected lipid compositions for DC have been examined (15). It was found that encapsulation efficiency for DC was higher with all examined types of liposomes than for tetracycline. The highest encapsulation rates for DC were achieved using cationic or neutral liposomes (15). Although pH is an important factor from the aspect of OTC/DC stability, in the literature there are no data reporting on the effect of pH or the type of hydrating solution on the encapsulation efficiency of tetracycline derivatives.

Present studies report results on the encapsulation efficiency of two tetracycline derivatives – OTC and DC – in liposomes with various lipid compositions including lecithin (LEC), α -L-dipalmitoyl-phosphatidylcholine (DPPC) and cholesterol (CHOL). The effects of pH (pH 4.0-8.0), liposomal cholesterol content and type of hydrating medium (phosphate buffer, glucose or mannitol solution) on the encapsulation rate of OTC and DC are also discussed. Encapsulation efficiencies for OTC and DC are compared to each other.

2. Materials and Methods

2.1. Preparation of liposomes

Multilamellar vesicles (MLVs) were prepared using the thin-film hydration method. Two milligrams of α -L-dipalmitoyl-phosphatidylcholine (DPPC) or lecithin (LEC) alone, or with cholesterol (CHOL) (70/30, mol/mol) were dissolved in absolute ethanol. The mixture was dried to thin-film under nitrogen stream, and any remaining solvent was removed from the lipid film in vacuum. The samples were stored in a desiccator overnight. Thin lipid films were hydrated above the main-transition temperature of DPPC, at $\sim 50^\circ\text{C}$. One mL of the solution of oxytetracycline hydrochloride (OTC) (MP Biomedicals Inc.) or doxycycline hydrochloride (DC) (MP Biomedicals Inc.) at a concentration of 0.1354 mg/mL was used for thin film hydration. The final lipid concentration was 2 mg/mL. The tested hydrating solutions, such as isotonic phosphate buffers (pH 6.0, 7.0, and 8.0) or glucose solutions (GLU) (5% m/m; pH 4.0, 6.0, 7.0, and 8.0) or mannitol solutions (MAN) (5% m/m; pH 4.0, 6.0, 7.0, and 8.0) were always freshly prepared. The isotonic phosphate buffer was prepared from Na_2HPO_4 and KH_2PO_4 and NaCl (Mallinckrodt Baker Inc.). The osmolarity of the solutions were measured by Osmomat

030-D osmometer (Medizintechnik Matel GmbH., Austria). The pH values of the GLU and MAN solutions were adjusted with diluted solutions of NaOH or HCl. The lipid/drug molar ratio for liposomes encapsulating OTC or DC was approximately 10:1. Control liposomes were hydrated with the appropriate solution without drug molecules. All lipid and cholesterol components were used without purification. All reagents were purchased from Sigma-Aldrich (St Louis, MO, USA) unless otherwise indicated.

2.2. Measurement of encapsulation efficiency

Freshly prepared OTC-, or DC-liposomes (400 μL) were centrifuged with a Galaxy 16 DH eppendorf centrifuge (2×10 min, $13,000 \times g$) through Nanosep 10K Omega Centrifugal Filter Devices (PALL Life Science Inc.) with a cut-off value of 10 kDa. The concentrations of OTC or DC in the filtrate, -representing the amounts of OTC or DC not encapsulated within the liposomes-, were determined by spectrophotometry (Genesys 10UV, Thermo Electron Corporation, NY, USA). (Wavelengths: 354 nm for solutions with a pH between 4.0 and 6.0; 361 nm for solutions with a pH of 7.0; and 369 nm for solutions with a pH of 8.0 for OTC and 347 nm for solutions with a pH between 4.0 and 6.0; 348 nm for solutions with a pH of 7.0 and 8.0 for DC). The absorbance values for hydrating solutions containing OTC or DC (0.1354 mg/mL) served as 100% for the encapsulation efficiency determinations. Each liposomal samples were measured at least in 3 replicates, and mean and standard deviation (S.D.) values were calculated. For data analysis statistical *t*-test were used with a significance level of 0.05.

2.3. Zeta-potential measurements

The zeta-potentials of liposomes were determined at a lipid concentration of 0.5 mg/mL. Samples were diluted with the appropriate freshly filtrated (0.2 μm pore size, Corning, Corning Incorporated, Germany) solution before the measurement. The measurements were carried out with a Zetasizer 3000 HSA (Malvern Instruments, UK).

3. Results and Discussion

According to the special requirements for the ophthalmic and parenteral formulations, our liposomal dosage forms satisfy the criteria of osmolarity and pH as previously described (16). The pH of the GLU and MAN solutions were adjusted to the required value (pH 4.0, 6.0, 7.0, and 8.0) after addition of OTC or DC. The presence of lipids does not have a significant impact on the pH value of the hydrating solution. The osmolarity of the samples hydrated with phosphate buffer (pH 6.0, 7.0, and 8.0) were approximately 310 mmol/L.

The GLU and MAN solutions are widely used and accepted in pharmaceutical formulations and both are well tolerated by the patients. The concentration of the antibiotics, OTC or DC, in our liposomal formulations (0.1354 mg/mL), was within the recommended range used in the antimicrobial therapy. For the sake of comparison, the marketed product ("Doxycycline for Injection USP" supplied as a sterile lyophilized powder) must be diluted with the given solvent(s) in order to provide a final DC concentration between 0.1 to 1.0 mg/mL (17).

Although for intravenous applications small unilamellar vesicles (SUVs) (diameter < 100 nm) are recommended, for these studies only multilamellar vesicles (MLVs) were prepared and evaluated. Our preliminary experiments with MLVs and SUVs showed only a slight (1-5%) difference in the encapsulation rates for the same drug molecule under identical conditions. Thus, on the basis of the data determined for MLVs one can have expectations how to formulate SUVs for the purpose of intravenous applications with relative high encapsulation efficiency.

There was no pH-dependent difference in the encapsulation efficiencies for OTC in phosphate buffer in both liposomal types (LEC, DPPC) when determined at pH 6.0 and 7.0 (Table 1). However, at pH 8.0 the encapsulation efficiencies were significantly different ($p < 0.05$), from that measured at lower pH values (pH 6.0 and 7.0) for the same liposomal composition. This finding is consistent with the reported pK_a values of 3.6, 7.5, and 9.4 for OTC (18). On the basis of these pK_a values, OTC molecules are positively charged at pH values below 3.6, they are present in zwitterionic form in the pH range of 3.6 to 7.5, and they bear one negative charge in the pH range of 7.5 to 9.4, while they have two negative charges at higher pH values than 9.4. At the pH-values examined in our study OTC is in zwitterionic form at pH 6.0 and 7.0, while it bears a negative charge at pH 8.0. The encapsulation efficiency seems to depend on the molecular form of the OTC. Interestingly, LEC encapsulates more, while DPPC less from the negative form of OTC than from the zwitterionic OTC molecules. It is important to remark, that according to our surface potential measurements the surface charge of OTC-free LEC and OTC-free DPPC liposomes in phosphate buffer is neutral or slightly positive (~0-4 mV). The value of the surface potential measured does not significantly depend on the pH value of the hydrating phosphate buffer (19). Thus, the difference observed between the encapsulation rates at higher (pH 8.0) and lower pH-values (pH 6.0 and 7.0) may be explained with the different membrane rigidities observed for LEC and DPPC. The membrane rigidity is an important factor: according to our measuring method, the term and value of the encapsulation efficiency reflect not only the amount of drug enclosed into the inner aqueous volume of liposomal vesicles

but also the amount of drug molecules that is more or less immersed into the liposomal bilayer(s) or weakly bounded to it. Excluding the special molecular interactions between lipids and OTC/DC, the amount of encapsulated OTC/DC would be proportional to the internal volume of the MLVs. According to our earlier electron paramagnetic resonance (EPR) spectroscopy measurements with MLVs (lipid concentration of 2 mg/mL), the inner/encapsulated volume of liposomes is approximately 2% of the total sample volume (19). The encapsulation efficiency data for the OTC- and DC-liposomes (data varying between 7.8% and 52.5%) (Tables 1-4) proved the accumulation of OTC/DC in the liposomes: a) in the lipid bilayer, b) attached to the liposomal surface with weak molecular interactions or c) in the inner aqueous volume.

The presence of CHOL has only a slight impact on the encapsulation rate determined for OTC containing LEC liposomes (Table 1). The results with the mixed liposomes (DPPC/CHOL 70/30 and LEC/CHOL 70/30) can be explained by the recognized feature of CHOL making the fluid bilayers more rigid and the rigid membranes (such as DPPC) more fluid. It is expected that the presence of CHOL in DPPC in 30% (mol/mol) concentration – at room temperature that is below the phase transition temperature of DPPC – makes the DPPC bilayer more fluid, similarly to the fluidity of LEC liposomes with unsaturated chains. Therefore, the addition of CHOL to DPPC results in a liposomal membrane that is more similar to the LEC liposomal membrane from the aspect of membrane fluidity and encapsulation efficiency, too.

For DC in phosphate buffers LEC showed higher encapsulation efficiencies than DPPC – at each pH value examined (Table 2). It can be supposed that the fluid structure of LEC allows DC to immerse (deeper) to the liposomal membrane.

Table 1. Encapsulation efficiency values for OTC in phosphate buffers with various lipid composition and various pH values (pH 6.0, 7.0, and 8.0)

pH	OTC encapsulation efficiency (%) (mean ± S.D.)			
	LEC	DPPC	LEC/CHOL 70/30	DPPC/CHOL 70/30
6.0	14.94 ± 3.34	23.23 ± 1.19	12.40 ± 2.25	8.68 ± 4.52
7.0	14.46 ± 2.10	24.10 ± 2.67	13.27 ± 0.50	7.77 ± 5.15
8.0	20.12 ± 0.42	12.97 ± 2.48	21.26 ± 1.71	16.83 ± 3.29

Table 2. Encapsulation efficiency values for DC in phosphate buffers with various lipid composition and various pH values (pH 6.0, 7.0, and 8.0)

pH	DC encapsulation efficiency (%) (mean ± S.D.)	
	LEC	DPPC
6.0	24.30 ± 2.12	15.98 ± 2.64
7.0	17.88 ± 3.16	16.18 ± 2.63
8.0	31.96 ± 3.07	16.29 ± 1.53

Table 3. Encapsulation efficiency values for OTC in glucose 5% m/m (GLU) and mannitol 5% m/m (MAN) solutions into LEC and DPPC liposomes at various pH values (pH 4.0, 6.0, 7.0, and 8.0)

pH	OTC encapsulation efficiency (%) (mean \pm S.D.)			
	LEC GLU	DPPC GLU	LEC MAN	DPPC MAN
4.0	11.38 \pm 1.12	20.99 \pm 2.98	16.27 \pm 0.10	24.09 \pm 0.65
6.0	13.78 \pm 5.88	16.98 \pm 1.44	10.45 \pm 4.32	10.45 \pm 4.32
7.0	10.23 \pm 1.62	8.06 \pm 0.36	16.19 \pm 3.44	17.94 \pm 2.76
8.0	38.18 \pm 3.31	38.72 \pm 0.78	15.43 \pm 1.54	12.99 \pm 5.05

Table 4. Encapsulation efficiency values for DC in glucose 5% m/m (GLU) and mannitol 5% m/m (MAN) solutions into LEC and DPPC liposomes at various pH values (pH 4.0, 6.0, 7.0, and 8.0)

pH	OTC encapsulation efficiency (%) (mean \pm S.D.)			
	LEC GLU	DPPC GLU	LEC MAN	DPPC MAN
4.0	46.16 \pm 2.06	23.85 \pm 6.17	52.18 \pm 0.38	44.54 \pm 1.06
6.0	42.10 \pm 2.10	24.28 \pm 0.30	48.72 \pm 3.81	39.47 \pm 7.27
7.0	38.21 \pm 6.89	28.31 \pm 4.79	38.20 \pm 8.27	30.36 \pm 1.92
8.0	42.84 \pm 1.14	21.20 \pm 3.95	44.83 \pm 2.93	52.47 \pm 6.45

OTC and DC differ in their chemical structures only by a hydroxyl group (Figure 1), thus OTC possesses more hydrophilic character than DC. According to our earlier experience, small changes in the chemical structure (*e.g.* the introduction of a methoxy group, similarly to the introduction of a hydroxyl group in our case) can result in pronounced alterations in the molecular interactions between the drug and liposomal membranes, thus influencing the encapsulation rates (20). It can give explanation to the fact, that DC can be more successfully encapsulated into LEC liposomes at each examined pH value. Similarly, as observed for OTC, in LEC at pH 8.0 the encapsulation efficiency for DC is higher than at pH 6.0 and 7.0. It is in coincidence with the pK_a values of 3.4, 7.7, and 9.3 determined for DC (21).

Evaluating the effects of the hydrating buffers on the encapsulation efficiency it can be concluded, that the use of non-ionic hydrating solutions (GLU or MAN) results in higher encapsulation efficiencies than the use of ionic phosphate buffers. In phosphate buffer the highest encapsulation efficiencies of $24.10 \pm 2.67\%$ and $31.96 \pm 3.07\%$, while in the non-ionic solutions the encapsulation efficiency values of $38.72 \pm 0.78\%$ and $52.47 \pm 6.45\%$ for OTC and DC were achieved, respectively (Tables 1-4). It was also observed that employing the non-ionic hydrating solutions, (GLU or MAN), instead of the ionic phosphate buffer can lead to a significant increase in the OTC/DC encapsulation efficiency. When GLU or MAN is used instead of phosphate buffer, the encapsulation efficiency can be enhanced by approximately two to three times in case of the LEC and DPPC liposomes (Tables 1-4). The

ions of the phosphate buffer and the non-dissociated molecules of the non-ionic hydrating solutions (*e.g.* GLU or MAN) behave in different ways in the environment of liposomal membranes, thus influencing the molecular interactions between drugs and lipids in a different manner. While the charged ions can "cover" and "mask" the original charge/surface potential of liposomal membranes, the GLU or MAN molecules do not have a significant impact on it. The ionic hydrating solutions do not allow to manifest the original surface charge of the bilayers and can influence the molecular interactions between the drug and lipid molecules. However, in GLU and MAN the original surface charge of the MLVs – through weak electrostatic interactions – can have a contribution to the relative high encapsulation efficiency for OTC/DC (19).

When comparing the encapsulation rates for OTC and DC in non-ionic hydrating solutions, it can be stated that DC can be encapsulated more effectively than OTC (Tables 3 and 4). The observation is possibly due to the difference in the chemical structures of the two antibiotics (Figure 1) as explained above.

On the basis of the results it can be stated that LEC encapsulates more – or at least not significantly less – DC than does DPPC at all pH values examined, and in all kinds of hydrating solutions used (phosphate buffer, GLU or MAN) (Tables 2 and 4). When considering the LEC liposomes, a wide variety of fatty acid chains (saturated and unsaturated, with various chain lengths) can ensure the encapsulation of DC molecules, leading to higher encapsulation rates. These data demonstrate that the liposomal encapsulation of DC requires LEC as the optimal lipid constituent.

When designing the parameters for encapsulating the drugs OTC/DC, care must be taken to choose the right pH value. It is known that the tetracyclines (such as OTC and DC) are more stable in the acidic pH range than at higher pH values (2-5). Thus a lower (acidic) pH seems to be the optimal choice. Taking both aspects (high encapsulation efficiency and higher drug stability at lower pH) into consideration, the liposomal compositions denoted with shadow in Tables 1-4 are recommended for the preparation of an optimal OTC/DC containing liposomal dosage form.

4. Conclusion

Based on our encapsulation efficiency studies and on the drug stability considerations it can be concluded that for OTC/DC encapsulation the use of non-ionic solutions (*e.g.* GLU) is the most promising. However, the use of GLU or MAN for hydration may increase the possibility of microbiological contamination of the liposomal preparations during storage. Therefore, it is necessary to lyophilize the liposomal samples for storage, and to rehydrate the samples before their therapeutic use. In consistence with the different

membrane rigidity values for LEC vs. DPPC the rate of the drug release for OTC and DC is also expected to be different in case of LEC and DPPC (22,23).

Acknowledgements

These studies were supported in part by research funds from the National Institute of Health (Grant #: 5 U01 NS058035-02) and the Robert A. Welch Foundation (x-0011) at Sam Houston State University.

References

- Tally FT, Ellestad GA, Testa RT. Glycocyclines: a new generation of tetracyclines. *J Antimicrob Chemother.* 1995; 35:449-452.
- Adriana MD, Michael KS. The kinetic of oxytetracycline degradation in deionized water under varying temperature, pH, light, substrate, and organic matter. *J Aquat Anim Health.* 2000; 12:246-253.
- Injak R, Djordjevic-Milic V, Srdjenovic B. Thermostability testing and degradation profiles of doxycycline in bulk, tablets, and capsules by HPLC. *J Chrom Sci.* 2007; 45:623-628.
- Liang Y, Denton MB, Bates RB. Stability studies of tetracycline in methanol solution. *J Chromatogr A.* 1998; 827:45-55.
- Mitscher LA. The chemistry of the tetracycline antibiotics; Medical Research Series, Vol. 9. Marcel Dekker, New York, NY, USA, 1978.
- Bartholomew RS, Reid BJ, Cheesbrough MJ, Macdonald M, Galloway NR. Oxytetracycline in the treatment of ocular rosacea: a double-blind trial. *Br J Ophthalmol.* 1982; 66:386-388.
- Brussieux J, Boisivon A, Théron HP, Faidherbe C, Machado N, Michelon B. Prevention of neonatal conjunctivitis. A comparative clinical and bacteriologic study of 2 eyedrops: silver nitrate and oxytetracycline chlorhydrate. *Ann Pediatr.* 1991; 38:637-641.
- Guzey M, Aslan G, Ozardali I, Basar E, Satici A, Karadede S. Three-day course of oral azithromycin vs topical oxytetracycline/polymyxin in treatment of active endemic trachoma. *Jpn J Ophthalmol.* 2000; 44:387-391.
- Eastmann TG, George LW, Hird DW, Thurmond MC. Combined parenteral and oral administration of oxytetracycline for control of infectious bovine keratoconjunctivitis. *J Am Vet Assoc.* 1998; 212:560-563.
- Ward DA, Clark ES. Ocular pharmacology. *Vet Clin North Am Food Anim Pract.* 1991; 7:779-791.
- Izer K, Török I, Pintér-Magyar G. Stability of oxytetracycline in eye-drops, prepared in pharmacies. *Acta Pharm Hung.* 1994; 64:63-66.
- Sah H. Degradation patterns of tetracycline antibiotics in reverse micelles and water. *Biomed Chromatogr.* 2006; 20:1142-1149.
- Okerman L, Van Hende J, De Zutter L. Stability of frozen stock solutions of beta-lactam antibiotics, cephalosporins, tetracyclines and quinolones used in antibiotic residue screening and antibiotic susceptibility testing. *Anal Chim Acta.* 2007; 586:284-288.
- Pinto-Alphandary H, Andremont A, Couvreur P. Targeted delivery of antibiotics using liposomes and nanoparticles: research and applications. *Int J Antimicrob Agents.* 2000; 13:155-168.
- Sangaré L, Morisset R, Omri A, Ravaoarino M. Incorporation rates, stabilities, cytotoxicities and release of liposomal tetracycline and doxycycline in human serum. *J Antimicrob Chemother.* 1998; 42:831-834.
- Völker-Dieben HJ, Kok-Van Alphen CC, Hollander CC, Kruit PJ, Batenburg K. The palliative treatment of the dry eye. *Documental Ophthalmol.* 1987; 67:221-227.
- Bedford Laboratories. Doxycycline for injection. 2004; USP, DIV-DCY-P03.
- Tavares MFM, McGuffin VL. Separation and characterization of tetracycline antibiotics by capillary electrophoresis. *J Chromatogr A.* 1994; 686:129-142.
- Budai M, Szabó Z, Zimmer A, Szögyi M, Gróf P. Studies on molecular interactions between nalidixic acid and liposomes. *Int J Pharm.* 2004; 279:67-79.
- Budai M, Szabó Z, Szogyi M, Gróf P. Molecular interactions between DPPC and morphine derivatives: a DSC and EPR study. *Int J Pharm.* 2003; 250:239-250.
- Sun XX, Aboul-Enein HY. Internal solid contact sensor for the determination of doxycycline hydrochloride in pharmaceutical formulation. *Talanta.* 2002; 58:387-396.
- Anderson M, Omri A. The effect of different lipid components on the *in vitro* stability and release kinetics of liposome formulations. *Drug Deliv.* 2004; 11:33-39.
- Budai L, Hajdú M, Budai M, Gróf P, Béni S, Noszá B, Klebovich I, Antal I. Gels and liposomes in optimized ocular drug delivery: Studies on ciprofloxacin formulations. *Int J Pharm.* 2007; 343:34-40.

(Received January 23, 2009; Accepted February 9, 2009)

Original Article

Study of the analgesic, anti-inflammatory, and gastric effects of gabapentin

Omar M. E. Abdel-Salam*, Amany A. Sleem

Department of Pharmacology, National Research Centre, Cairo, Egypt.

ABSTRACT: Gabapentin, a drug used to treat neuropathic pain, was evaluated in models of acute nociceptive pain, in instances of haloperidol-induced catalepsy, carrageenan-induced paw edema, gastric lesions caused by indomethacin or ethanol, and gastric acid secretion in rats. Reaction time in a hot plate assay was delayed by gabapentin. The antinociceptive effect of the drug was produced with a dose of 12.5 mg/kg and a maximal increase in hot plate latency of 68% 1 h after drug administration was produced at 100 mg/kg. Gabapentin (25, 50 or 100 mg/kg) caused a significant rise in current threshold in a tail electrical stimulation test in mice, resulting in values of 20, 30, and 60.5% vs. control values, 1 h post-dosing. With the agent, the duration of paw licking following intraplantar capsaicin injection decreased in a dose-dependent manner. In contrast, gabapentin failed to have antinociceptive action in a mouse acetic-acid-induced writhing assay. The drug (12.5-50 mg/kg) increased the duration of catalepsy induced by haloperidol by 33.5, 47.4, and 53.2%, respectively. It had an anti-inflammatory effect at doses of 25 or 50 mg/kg. Gabapentin (12.5-50 mg/kg) reduced the number and severity of gastric mucosal lesions induced by subcutaneous indomethacin (20 mg/kg) or intragastric 96% ethanol, but at doses of 50 and 100 mg/kg it increased gastric acid secretion. In conclusion, gabapentin decreased thermal, electrical, and chemogenic pain but not visceral pain and had a gastric protective effect.

Keywords: Gabapentin, Pain, Gastric lesions, Mice, Rat

1. Introduction

Gabapentin, 1-(aminomethyl)cyclohexane acetic

**To whom correspondence should be addressed:*

Dr. Omar M. E. Abdel-Salam, Department of Pharmacology, National Research Centre, Cairo, Egypt; e-mail: omasalam@hotmail.com

acid, is a structural analog of γ -aminobutyric acid (GABA), which was initially introduced in 1994 as an antiepileptic drug used especially to treat partial seizures. Despite the fact that gabapentin is structurally related to the neurotransmitter GABA, there is no conclusive evidence yet that gabapentin blocks GABA uptake or metabolism, that it binds to GABAA or GABAB receptors, or that it has any GABA-mimetic action (1,2).

In experimental animal models of mechanical hyperalgesia and mechanical/thermal allodynia, gabapentin has been reported to have a potent inhibitory effect (3-7). For example, the drug decreased tactile hypersensitivity and mechanical and cold hypersensitivity due to spinal cord compression in rats or due to paclitaxel- and vincristine-administration (8-10), it attenuated the second phase of nociceptive responses in a formalin test (11), it lessened mechanical hypersensitivity induced by intraplantar capsaicin (12), and it reduced mechanical hypersensitivity in a model of varicella zoster virus-associated hypersensitivity (13).

In humans, gabapentin has become increasingly popular as a treatment for chronic neuropathic pain. Clinical studies have shown that gabapentin is an effective analgesic in different types of neuropathic pain syndromes such as diabetic neuropathy (14), postherpetic neuralgia (15), trigeminal neuralgia (16), painful neuropathy resulting from HIV infection (17), cancer pain (18), fibromyalgia (19), pain following a burn injury (20), and complex regional pain syndromes (21). Although the exact molecular mechanism of action by which gabapentin reduces pain is not yet known, evidence suggests that the $\alpha 2\delta 1$ auxiliary subunit of voltage-gated calcium channels are the target for this drug's actions (22).

The aim of the present study was to investigate the effect of gabapentin on acute nociception and acute inflammation induced in rats by subplantar carrageenan injection. In addition, the effects of the compound on haloperidol-induced catalepsy, gastric acid secretion, and gastric mucosal damage caused by indomethacin or ethanol were evaluated.

2. Materials and Methods

2.1. Animals

Sprague-Dawley strain rats weighing 120-130 g or Swiss albino mice weighing 20-25 g of body weight were used and housed under standardized conditions at the National Research Centre, Cairo, Egypt with free access to food and water. Experiments were performed between 900 and 1,500 h. All animal procedures were performed in accordance with the Ethics Committee of the National Research Centre and followed the recommendations for the proper care and use of laboratory animals (NIH publication No. 85-23, revised 1985). Equal-sized groups of 6 rats or 6 mice were used in all experiments. Gabapentin doses in this study were based upon human doses after converting to those for rats according to Paget and Barnes conversion tables (23).

2.2. Drugs and reagents

Gabapentin (Delta Pharma, Cairo, Egypt), carrageenan, capsaicin (Sigma-Aldrich, St Louis, MO, USA), indomethacin, and haloperidol (Kahira Pharm & Chem. IND Co., Cairo, Egypt) were used. Stock solutions of capsaicin (10 mg/mL) contained 10% ethanol, 10% Tween 80, and 80% saline solution. Analytical-grade glacial acetic acid (Sigma-Aldrich) was diluted with pyrogen-free saline to provide a 0.6% solution for *i.p.* injection. All drugs were dissolved in isotonic (0.9% NaCl) saline solution immediately before use, except for indomethacin, which was dissolved in a 5% solution of sodium bicarbonate.

2.3. Hot-plate assay

A hot-plate test was performed using an electronically controlled hotplate (Ugo Basile, Comerio, Italy) heated to 53°C ($\pm 0.1^\circ\text{C}$). Each mouse was placed unrestrained on the hot plate for baseline measurement just prior to saline or drug administration. Different groups of mice ($n = 6/\text{group}$) were given gabapentin (12.5, 25, 50 or 100 mg/kg, 0.2 mL, intraperitoneally) or saline (control). Measurements were then taken 30 and 60 min after drug administration. The experimenter was blind to doses. Latency to licking a hind paw or jumping from the apparatus was recorded for the control and drug-treated groups. The cut-off time was 30 sec.

2.4. Tail electric stimulation test

Groups of mice ($n = 6/\text{group}$) were given gabapentin (12.5, 25, 50 or 100 mg/kg, *i.p.*) or saline (control). The minimum current required to elicit vocalization upon electrical stimulation of the tail was determined for the control and drug-treated groups 2 h post-treatment (24).

Electrical stimulation of the tail was applied by means of the Pulse generator 57800-001 (Eugo Basil EXT Unit) (Frequency 50 pulse/sec, shock duration 2 sec).

2.5. Capsaicin-induced hind paw licking

Gabapentin (12.5, 25, 50 or 100 mg/kg, *i.p.*) or saline was administered 60 min before injection of capsaicin (1.6 $\mu\text{g}/\text{paw}$; 25 μL) under the skin of the dorsal surface of the right hind paw. Observation started after capsaicin injection and lasted for 5 min. The time the animal spent licking the injected paw was determined using a stopwatch (25).

2.6. Acetic acid-induced writhing

Separate groups of 6 mice each were administered a vehicle (saline) or gabapentin 12.5, 25, 50 or 100 mg/kg; 0.2 mL, orally or intraperitoneally (*i.p.*). After 60 min of oral administration or 30 min of *i.p.* administration of gabapentin, mice received an *i.p.* injection of 0.6% acetic acid (0.2 mL) (26). The number of abdominal constrictions over 30 min following acetic acid injection was noted for the control and drug-treated groups.

2.7. Carrageenan-induced paw edema

Paw edema was induced by sub-plantar injection of 100 μL of 1% sterile λ -carrageenan in saline into the right hind paw of rats (27). The contralateral paw received an equal volume of saline. Paw volume was determined immediately before carrageenan injection and at selected times thereafter using a plethysmometer (Ugo Basile). The edema component of inflammation was quantified by measuring the paw volume (mL) at zero time (before carrageenan injection) and at 1, 2, 3, and 4 h after carrageenan injection; this value was then compared to the pre-injection value for each animal. Edema was expressed as a percentage change from control (pre-drug, zero time) values. The effect of systemic administration of gabapentin (25, 50 or 100 mg/kg, *s.c.*, 0.2 mL, $n = 6/\text{group}$) given 30 min. before induction of inflammation by subplantar carrageenan was studied. The control group of carrageenan-treated rats received an equal volume of saline 30 min. before subplantar carrageenan injection ($n = 6$ each).

In addition, the effect of concomitantly administered gabapentin and indomethacin on edema formation was investigated. Different groups of rats ($n = 6$ each) were administered indomethacin (20 mg/kg, *s.c.*) alone or concomitantly administered gabapentin (100 or 200 mg/kg, *i.p.*) 30 min before subplantar carrageenan. The control group of carrageenan-treated rats received an equal volume of saline (0.2 mL) before subplantar carrageenan injection ($n = 6$).

2.8. Rotarod testing

Motor performance in mice was measured as the latency to falling from an accelerating rotarod located over plates connected to an automatic counter (Ugo Basile). Mice were trained to remain on a rotating rod for 2 min as the rod rotated toward the animal. After the 2-min training period, the mice were administered a vehicle (saline) or gabapentin (50 or 100 mg/kg, *i.p.*) and 30 min later placed on the rotating rod as it accelerated from 4 to 40 rpm over 5 min; the time they were able to remain on the accelerating rod was noted (28). The cutoff time was 600 sec. The time was measured from the start of the acceleration period. The test was repeated 2 h after vehicle or drug injection. Six animals were used per dose and for the controls.

2.9. Haloperidol-induced catalepsy

Catalepsy, defined as a reduced ability to initiate movement and a failure to correct posture, was measured with a bar test. Mice were positioned so that their hindquarters were on the bench and their forelimbs rested on a 1 cm diameter horizontal bar 4 cm above the bench. The length of time the mouse maintained this position was recorded with a stopwatch for a maximum of 180 sec. This procedure was performed 30 min after haloperidol (2 mg/kg, *i.p.*) administration (29). Gabapentin (12.5, 25 or 50 mg/kg, *i.p.*) was concomitantly administered with haloperidol. Mice were judged to be cataleptic if they maintained this position for 30 sec or more.

2.10. Haloperidol-induced locomotor impairment

Mice were administered saline, haloperidol (2 mg/kg, *i.p.*), or haloperidol + gabapentin (25, 50 or 100 mg/kg, *i.p.*). Thirty min after treatment with drugs or the vehicle, mice were individually placed into a 40 cm³ activity monitor equipped with photoelectric detectors and the total number of horizontal beam interruptions (spontaneous locomotor activity) was counted over a 6 min period for each animal.

2.11. Gastric ulcerogenic studies

Gastric mucosal damage was induced in rats by administration of indomethacin (20 mg/kg, 0.2 mL, *s.c.*). The effect of gabapentin (12.5, 25 or 50 mg/kg, *i.p.*) administered at the time of indomethacin injection was studied. Food and water were provided *ad libitum*. In other experiments, the effect of gabapentin (12.5, 25 or 50 mg/kg, *i.p.*) on gastric damage caused by ethanol was evaluated. Rats fasted for 18 h but were allowed water *ad libitum*. They were administered either saline (control) or different doses of gabapentin 30 min prior to ethanol (96%, 1 mL, *p.o.*). Rats were sacrificed 24 h

after indomethacin or 1 h after ethanol administration. Their stomachs were removed and opened along the greater curvature; the stomachs were then rinsed with saline, extended on a plastic board, and examined for mucosal lesions. The number and severity of mucosal lesions were noted and lesions were scaled as described by Mózsik *et al.* (30).

2.12. Gastric acid secretion studies

Investigations were carried out in a pylorus-ligated rat model. Pylorus ligation was done under light ether anesthesia in rats that had fasted for 18 h with access to water *ad libitum*. Care was taken so as not to interfere with the blood supply to the stomach or duodenum. The abdominal wall was closed in layers with silk sutures. Rats then received either saline (0.2 mL/rat, *s.c.*, *n* = 6) (control) or different doses of gabapentin (50, 100, or 200 mg/kg, 0.2 mL/rat, *s.c.*, *n* = 6/group). Rats were sacrificed 4 h later. Gastric acid output was determined by titration to pH 7.0 with 0.01 N NaOH and H⁺ output expressed as $\mu\text{Eq}/4\text{ h}$.

2.13. Statistical analysis

Data are expressed as mean \pm SE. Data were analyzed by one-way analysis of variance, followed by a Tukey's multiple range test for *post hoc* comparison of group means. When there were only two groups, a two-tailed Student's *t* test was used. For all tests, effects with a probability of $p < 0.05$ were considered to be significant.

3. Results

3.1. Anti-nociceptive effects of gabapentin

3.1.1. Hot-plate assay

The reaction time on the hot plate was delayed by gabapentin. Gabapentin at doses of 12.5-100 mg/kg significantly increased hot-plate latency in the mouse hot plate test. The anti-nociceptive effect of the drug was produced with a 12.5 mg/kg and a maximal increase in hot-plate latency of 68% was noted 1 h after drug administration (Figure 1, Table 1).

3.1.2. Tail electric stimulation test

Gabapentin (25, 50 or 100 mg/kg) produced a significant rise in electrical current threshold in the tail stimulation test in rats; this rise was 20, 30, and 60.5% vs. control values, 1 h post-drug (Table 2).

3.1.3. Capsaicin-induced hind paw licking

The duration of paw licking following intraplantar capsaicin injection was reduced by gabapentin in

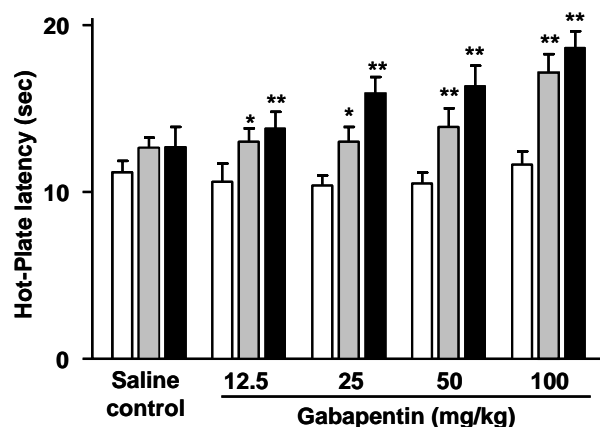


Figure 1. Basal (pre-drug, open column), 30 min (gray column) and 1 h (closed column) values of hot-plate latency (seconds) of saline (control) and gabapentin-treated mice. Each column represents mean \pm SE of 6 mice/group. * $p < 0.05$, ** $p < 0.01$ compared to the basal value.

Table 1. Anti-nociceptive activity of gabapentin in the hot-plate test in mice

Drugs	Latencies (sec) for nociceptive reaction after			% change	
	0 min (baseline)	30 min	1 h	30 min	1 h
Saline	11.2 \pm 0.66	12.65 \pm 0.61	12.7 \pm 1.2		
Gabapentin					
12.5 mg/kg	10.6 \pm 0.90	13.0 \pm 0.8*	13.8 \pm 1.0**	22.6	30.2
25 mg/kg	10.4 \pm 0.59	13.1 \pm 0.91*	15.8 \pm 1.1**	26.0	51.9
50 mg/kg	10.5 \pm 0.65	13.9 \pm 1.1**	16.35 \pm 1.0**	32.0	55.7
100 mg/kg	11.1 \pm 0.8	17.15 \pm 1.2**	18.65 \pm 1.0**	54.5	68.0

Shown are baseline (0 time) and drug-induced (30 min and 1 h measurements) latencies (in seconds) for the nociceptive reaction. Data are expressed as means and S.E.M. ($n = 6$ /group). Asterisks indicate a significant increase in nociceptive latencies (* $p < 0.05$, ** $p < 0.01$) compared to the baseline level of nociceptive reaction (Student's t test).

Table 2. Anti-nociceptive activity of gabapentin in the tail electric stimulation test in mice

Drugs	Electric current threshold (μ A)	% change
Saline	200.0 \pm 6.0	
Gabapentin		
12.5 mg/kg	221.3 \pm 18.3	10.6
25 mg/kg	240.3 \pm 16.1*	20.2
50 mg/kg	260.0 \pm 21.0*	30.0
100 mg/kg	320.0 \pm 20.0**	60.0

Shown are control and drug-induced changes for the nociceptive reaction. Data are expressed as means \pm SE. ($n = 6$ /group). * Significant rise in electrical current threshold (μ A) ($p < 0.05$) compared to the saline control group (One-way ANOVA, Duncan test).

a dose-dependent manner (by 17.8, 26.9, 37.4, and 40.8% after 12.5, 25, 50, and 100 mg/kg gabapentin, respectively) (Figure 2).

3.1.4. Acetic acid-induced writhing test

Visceral nociceptive behavior following *i.p.* administration of dilute acetic acid in mice was unaffected following oral or *i.p.* gabapentin administration (Table 3).

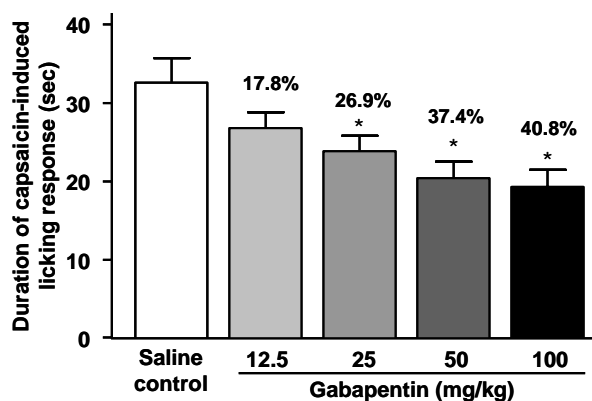


Figure 2. Effect of gabapentin on the duration of licking response to capsaicin injection in mice. Data represent mean values (\pm SE) and percent inhibition (%) compared to the control animals. Statistical differences vs. the control group are indicated by asterisks.

Table 3. Effect of gabapentin on the number of writhes in the acetic acid test in mice

Drugs	Number of abdominal constrictions/30 min	
	Oral	Intraperitoneal
Saline	63.5 \pm 3.7	70.3 \pm 6.2
Gabapentin		
12.5 mg/kg	54.8 \pm 2.6	81.0 \pm 7.6
25 mg/kg	50.0 \pm 3.7	77.0 \pm 7.2
50 mg/kg	49.5 \pm 4.2	82.0 \pm 6.7
100 mg/kg	67.0 \pm 4.3	78.9 \pm 5.1

Data are expressed as means \pm SE ($n = 6$ /group).

3.2. Anti-inflammatory effects of gabapentin

The administration of gabapentin inhibited carrageenin-induced paw edema (two-way ANOVA; treatment effect: $F_{3,80} = 57.1$; $p < 0.001$; time effect: $F_{3,80} = 42.6$; $p < 0.001$). Edema was significantly inhibited by all doses of gabapentin at all measured times (-26.2, -42.6, -34.6, and -34.9% for 25 mg/kg gabapentin vs. -26.2, -41.1, -36.6, and -35.6% for 50 mg/kg gabapentin and -16.7, -25, -22.1, and -22.2% for 100 mg/kg gabapentin at 1, 2, 3, and 4 h post-carrageenan, respectively) (Figure 3).

The group treated with the lower dose of the drug (25 mg/kg) exhibited significant suppression of edema compared to the group treated with 50 mg/kg 2 h post-carrageenan and compared to the group treated with 100 mg/kg at 2 h and 3 h after carrageenan injection, respectively (Figure 3). Therefore, the effect of concomitantly administered gabapentin at high doses of 100 or 200 mg/kg and indomethacin was examined for a possible modulating effect on indomethacin's anti-inflammatory effect.

Concomitant administration of gabapentin with indomethacin suppressed paw edema at all measured times (-36.7, -42.4, -43.7, and -44.4% for indomethacin vs. -33.4, -32.3, -38.4, and -37.6% for indomethacin + 100 mg/kg gabapentin and -35.5, -39.2, -39, and -36.1% for indomethacin + 200 mg/kg gabapentin at 1, 2, 3, and 4 h, respectively) (Figure 4). Two-way ANOVA revealed a significant main effect of treatment ($F_{3,80}$

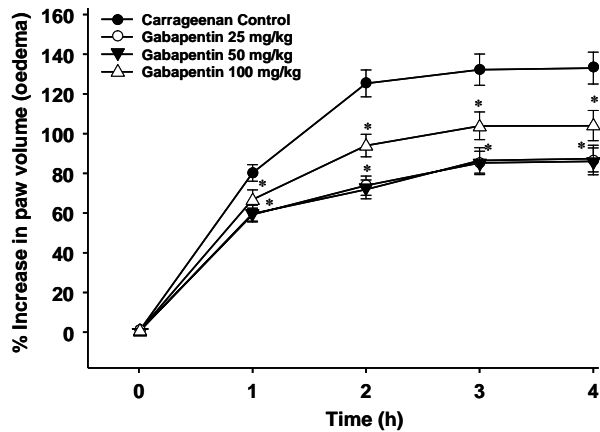


Figure 3. Effect of different doses of gabapentin on rat paw edema induced by carrageenan. Results are expressed as a percentage change from control (pre-drug) values, with each point representing the mean \pm SE of 6 rats/group. Asterisks indicate a significant change from the control group at the corresponding time.

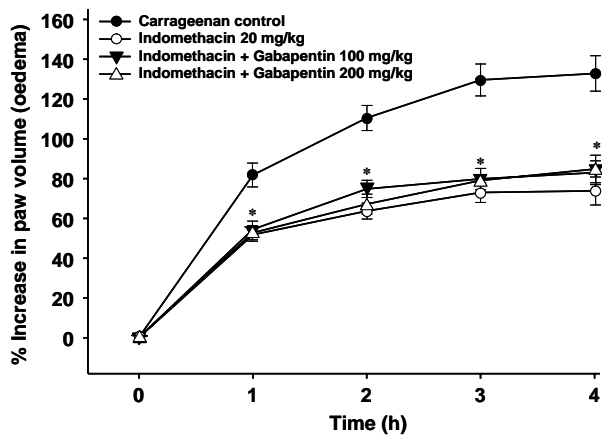


Figure 4. Effect of gabapentin on the antiedemic effect of indomethacin in the carrageenan paw edema assay in the rat. Results are expressed as a percentage change from control (pre-drug) values, with each point representing the mean \pm SE of 6 rats/group. Asterisks indicate a significant change from the control group at the corresponding time.

= 81.3; $p < 0.001$) and time ($F_{3,80} = 37.6$; $p < 0.001$). Post hoc comparisons showed significant inhibition of edema formation by indomethacin or indomethacin + gabapentin at all measured times.

3.3. Rotarod testing

Gabapentin did not produce any significant changes in mice with regard to rotarod performance (data not shown).

3.4. Effect of gabapentin on the duration of haloperidol-induced catalepsy

Haloperidol administered *i.p.* at a dose of 2 mg/kg produced a significant cataleptic response. The duration of haloperidol-induced catalepsy significantly increased 33.5, 47.4, and 53.2% as a result of 12.5, 25, and 50 mg/kg of gabapentin, respectively (Figure 5).

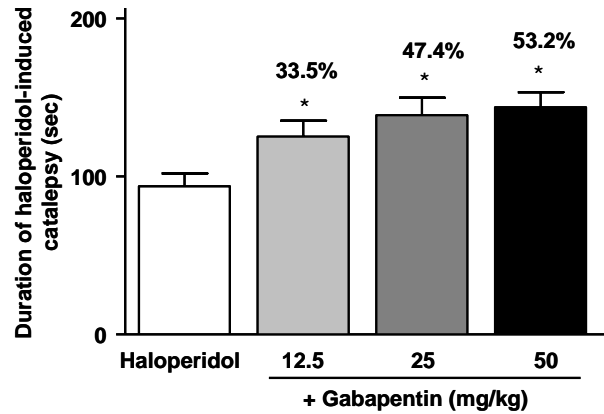


Figure 5. Effect of gabapentin on haloperidol-induced catalepsy in mice. Data represent mean values (\pm SE) of 6 mice per group and percent increase (%) compared to the control animals. Statistical differences vs. the control group are indicated by asterisks.

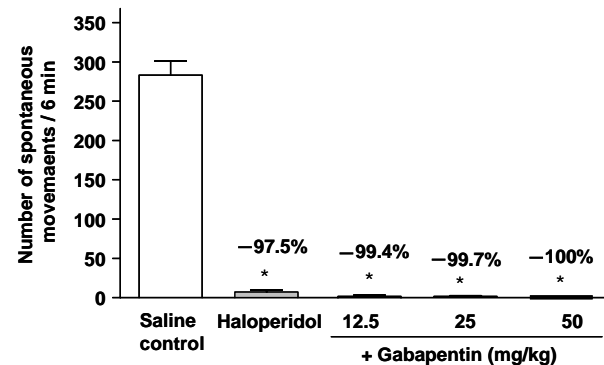


Figure 6. Effect of gabapentin on haloperidol-induced motor impairment in mice. Data represent mean values (\pm SE) of 6 mice per group and percent inhibition (%) compared to the control animals. Statistical differences vs. the control group are indicated by asterisks.

3.5. Effect of gabapentin on haloperidol-induced locomotor impairment

Spontaneous motor activity was markedly and significantly reduced in haloperidol-treated mice. Treatment with gabapentin resulted in a further reduction in motor activity (Figure 6).

3.6. Effect of gabapentin on gastric mucosal lesions caused by indomethacin or ethanol

Gabapentin (12.5-100 mg/kg) administered at the time of indomethacin injection or 30 min prior to ethanol (96%) prevented the development of gastric lesions caused by either ulcerogen in a dose-dependent manner (Figures. 7-10).

3.7. Effect of gabapentin on gastric acid secretion

Gabapentin (50-200 mg/kg) administered at the time of pylorus ligation increased gastric acid secretion; this effect was most marked with doses of 50 and 100 mg/kg (Table 4).

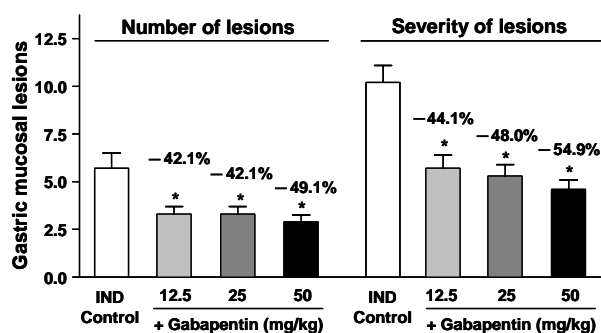


Figure 7. Effect of gabapentin on the number and severity of gastric lesions induced by indomethacin (IND) in rats. Results are expressed as mean values of 6 observations (\pm SE) and percent inhibition (%) compared to the control group. * $p < 0.05$ compared to the IND control.

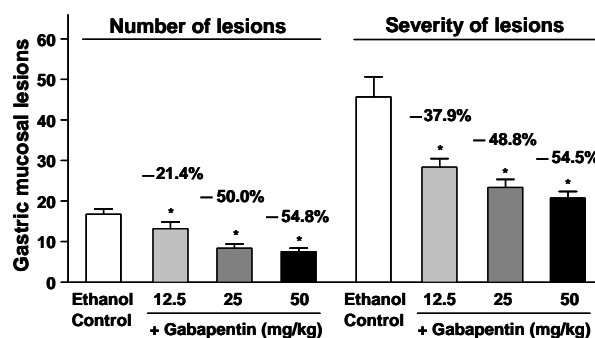


Figure 8. Effect of gabapentin on the number and severity of gastric lesions induced by ethanol in rats. Results are expressed as mean values of 6 observations (\pm SE) and percent inhibition (%) compared to the control group. * $p < 0.05$ compared to the ethanol control.



Figure 9. Gross appearance of rat gastric mucosa after treatment with indomethacin (upper) or indomethacin + gabapentin 100 mg/kg (lower).

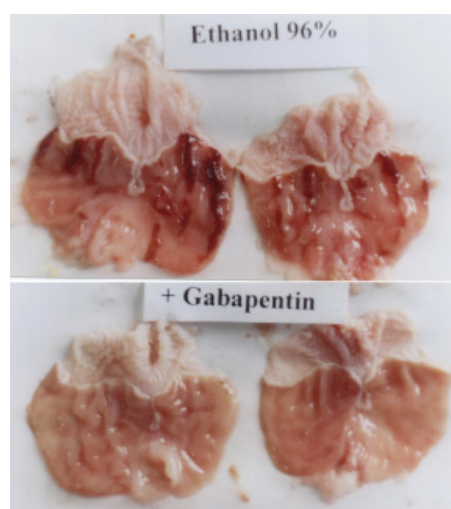


Figure 10. Gross appearance of rat gastric mucosa exposed to 96% ethanol (upper) or ethanol + gabapentin 100 mg/kg (lower).

Table 4. Effect of gabapentin on gastric acid secretion in pylorus-ligated rat

Drugs	Gastric volume (mL)	Gastric acid secretion (μ Eq/4 h)
Saline	2.65 \pm 0.3	142.5 \pm 8.2
Gabapentin		
50 mg/kg	3.38 \pm 0.6	242.5 \pm 13.6*
100 mg/kg	3.0 \pm 0.4	300.0 \pm 17.4*
200 mg/kg	2.8 \pm 0.4	153.8 \pm 6.9

Data are expressed as means \pm SE ($n = 6$ /group). * $p < 0.05$ vs. saline-treated group.

4. Discussion

Studies have demonstrated the analgesic and antiallodynic effects of gabapentin in models involving neuronal sensitization and nerve injury. The aim of the present study was to investigate the effect of gabapentin on acute nociceptive pain. Data from the present study indicates that the systemic administration of gabapentin resulted in antinociceptive effects in different acute pain models. The drug increased the nociceptive threshold

to thermal or electrical stimuli. In addition, chemogenic pain behavior induced by capsaicin injection in mice was markedly reduced by gabapentin. Other researchers have noted a reduction in mechanical hypersensitivity induced by intraplantar capsaicin with gabapentin (31). At doses that caused effective anti-nociception, the drug did not impair mouse performance as evaluated by the rotarod test, thus ruling out the confounding influence of a possible sedative effect. In the writhing test in mice, a widely used model of visceral inflammatory pain that involves the local release of prostacyclin (32), gabapentin administered *via* oral or systemic routes failed to alter the number of abdominal constrictions induced by acetic acid injection into the peritoneal cavity. Gabapentin (56 mg/kg) also had no effect on cyclophosphamide-induced cystitis in mice, a model of visceral pain (33). Other investigators, however, have reported a reduction in the number of writhes as a result of gabapentin (10-70 mg/kg, *p.o.*) (34).

Gabapentin is thought to act at supraspinal and intraspinal sites to induce antinociceptive responses

(35,36). Gabapentin has been shown to modulate brain c-Fos expression in surgical paw incision and to attenuate acute morphine-induced c-Fos expression in the rat striatum (37,38). The activation of brain areas involved in nociceptive processing indicates a supraspinal site of action for gabapentin (36). In the present study, the drug increased latency in hotplate tests, which are reported to detect antinociception mediated primarily by supraspinal mechanisms (39). The mechanism of the analgesic action of gabapentin is not known, but evidence suggest that the $\alpha 2\delta 1$ auxiliary subunit of voltage-gated calcium channels serves the target for the drug's actions (22), but acute inhibition of calcium currents by the drug is either very minor or absent (40). The analgesic effects of gabapentin might also involve inhibition of spinal release of substance P and CGRP (41) or of glutamate (42). There is also evidence to suggest that the antihyperalgesic and antiallodynic effects of gabapentin are mediated substantially by the descending noradrenergic system, resulting in the activation of spinal $\alpha 2$ -adrenergic receptors (35).

In the present study, gabapentin also reduced the inflammatory edematogenic response to subplantar carrageenan injection, with the lower doses of 25 and 50 mg/kg being more effective than the higher dose of 100 mg/kg. The effect of gabapentin was less than that of indomethacin. Gabapentin at high doses, however, is unlikely to affect the anti-inflammatory effect of non-steroidal anti-inflammatory drugs *e.g.*, indomethacin.

Catalepsy occurs following high dopamine D2 receptor blockade by a typical antipsychotic drug like haloperidol (29). Haloperidol-induced catalepsy is a behavioral predictor of susceptibility to extrapyramidal symptoms (43). In the present study, gabapentin increased the duration of catalepsy in a dose-related manner. In patients with advanced Parkinsonism, improvement (though non-significant) of rigidity, bradykinesia, and tremors was noted (44). Other researchers have found that gabapentin improved Parkinsonian symptoms and motor response following levodopa, although this improvement was not reflected in the daily motor status of patients. Levodopa-induced dyskinesias remained unchanged (45). Improvement in antipsychotic-induced akathisia upon treatment with gabapentin has also been reported (46). In patients on gabapentin treatment, somnolence and dizziness are observed side effects (47), but there are recent reports of dyskinesia (48) or even hemichorea (49) caused by gabapentin, and this issue warrants further study. Since there is no clear evidence that gabapentin has GABA-mimetic action (1,2), gabapentin's effects on extrapyramidal motor symptoms are unlikely to be mediated *via* the GABA neurotransmitter system. Spinal cholinergic activation was reported after oral administration of gabapentin in rats (50). Since muscarinic acetylcholine receptor

antagonists may contribute to the reduction of catalepsy (43), gabapentin's effect on striatal cholinergic or other neurotransmitter systems may account for the accentuation of haloperidol catalepsy following gabapentin in the present study.

Findings of the present study also indicate that gabapentin has a gastric protective effect. Acute gastric mucosal lesions induced by indomethacin or ethanol in the rat decreased in a dose-dependent manner as a result of concomitant administration. Gabapentin increased gastric acid secretion in pylorus-ligated rats, indicating that its gastric mucosal protective properties are unlikely to include an effect on gastric acid.

References

1. Jensen AA, Mosbacher J, Elg S, Lingenhoehl K, Lohmann T, Johansen TN, Abrahamsen B, Mattsson JP, Lehmann A, Bettler B, Bräuner-Osborne H. The anticonvulsant gabapentin (neurontin) does not act through gamma-aminobutyric acid-B receptors. *Mol Pharmacol.* 2002; 61:1377-1384.
2. Bennett MI, Simpson KH. Gabapentin in the treatment of neuropathic pain. *Palliat Med.* 2004; 18:5-11.
3. Abdi S, Lee DH, Chung JM. The anti-allodynic effects of amitriptyline, gabapentin, and lidocaine in a rat model of neuropathic pain. *Anesth Analg.* 1998; 87:1360-1366.
4. Cho HS, Kim MH, Choi DH, Lee J, Gwak MS, Hahm TS. The effect of intrathecal gabapentin on mechanical and thermal hyperalgesia in neuropathic rats induced by spinal nerve ligation. *J Korean Med Sci.* 2002; 17:225-229.
5. Yasuda T, Miki S, Yoshinaga N, Senba E. Effects of amitriptyline and gabapentin on bilateral hyperalgesia observed in an animal model of unilateral axotomy. *Pain.* 2005; 115:161-170.
6. Meymandi MS, Sepehri G, Mobasher M. Gabapentin enhances the analgesic response to morphine in acute model of pain in male rats. *Pharmacol Biochem Behav.* 2006; 85:185-189.
7. Cheng JK, Chen CC, Yang JR, Chiou LC. The antiallodynic action target of intrathecal gabapentin: Ca^{2+} channels, KATP channels or *N*-methyl-d-aspartic acid receptors? *Anesth Analg.* 2006; 102:182-187.
8. Hama A, Sagen J. Behavioral characterization and effect of clinical drugs in a rat model of pain following spinal cord compression. *Brain Res.* 2007; 1185:117-128.
9. Coderre TJ, Kumar N, Lefebvre CD, Yu JS. A comparison of the glutamate release inhibition and anti-allodynic effects of gabapentin, lamotrigine, and riluzole in a model of neuropathic pain. *J Neurochem.* 2007; 100:1289-1299.
10. Xiao W, Boroujerdi A, Bennett GJ, Luo ZD. Chemotherapy-evoked painful peripheral neuropathy: analgesic effects of gabapentin and effects on expression of the alpha-2-delta type-1 calcium channel subunit. *Neuroscience.* 2007; 144:714-720.
11. Munro G, Erichsen HK, Mirza NR. Pharmacological comparison of anticonvulsant drugs in animal models of persistent pain and anxiety. *Neuropharmacology.* 2007; 53:609-618.
12. Joshi SK, Hernandez G, Mikusa JP, Zhu CZ, Zhong C,

- Salyers A, Wismer CT, Chandran P, Decker MW, Honore P. Comparison of antinociceptive actions of standard analgesics in attenuating capsaicin and nerve-injury-induced mechanical hypersensitivity. *Neuroscience*. 2006; 143:587-596.
13. Hasnie FS, Breuer J, Parker S, Wallace V, Blackbeard J, Lever I, Kinchington PR, Dickenson AH, Pheby T, Rice AS. Further characterization of a rat model of varicella zoster virus-associated pain: Relationship between mechanical hypersensitivity and anxiety-related behavior, and the influence of analgesic drugs. *Neuroscience*. 2007; 144:1495-1508.
 14. Backonja M, Beydoun A, Edwards KR, Schwartz SL, Fonseca V, Hes M, LaMoreaux L, Garofalo E. Gabapentin for the symptomatic treatment of painful neuropathy in patients with diabetes mellitus: a randomized controlled trial. *JAMA*. 1998; 280:1831-1836.
 15. Singh D, Kennedy DH. The use of gabapentin for the treatment of postherpetic neuralgia. *Clin Ther*. 2003; 25:852-889.
 16. Pöllmann W, Feneberg W. Current management of pain associated with multiple sclerosis. *CNS Drugs*. 2008; 22:291-324.
 17. Newshan G. HIV neuropathy treated with gabapentin. *AIDS*. 1998; 12:219-221.
 18. Berger A, Dukes E, Mercadante S, Oster G. Use of antiepileptics and tricyclic antidepressants in cancer patients with neuropathic pain. *Eur J Cancer Care*. 2006; 15:138-145.
 19. Crofford LJ. Pain management in fibromyalgia. *Curr Opin Rheumatol*. 2008; 20:246-250.
 20. Gray P, Williams B, Cramond T. Successful use of gabapentin in acute pain management following burn injury: a case series. *Pain Med*. 2008; 9:371-376.
 21. Tan AK, Duman I, Taÿkaynatan MA, Hazneci B, Kalyon TA. The effect of gabapentin in earlier stage of reflex sympathetic dystrophy. *Clin Rheumatol*. 2007; 26:561-565.
 22. Maneuf YP, Luo ZD, Lee K. $\alpha 2\delta$ and the mechanism of action of gabapentin in the treatment of pain. *Semin Cell Dev Biol*. 2006; 17:565-570.
 23. Paget GE, Barnes JM. Toxicity tests. In: *Evaluation of Drug Activities Pharmacometrics* (Laurence DR, Bacharach AL, eds.). Academic Press, London and New York, 1964; pp. 1-135.
 24. Michael-Titus A, Costentin J. Analgesic effects of metapramine and evidence against the involvement of endogenous enkephalins in the analgesia induced by tricyclic antidepressants. *Pain*. 1987; 31:391-400.
 25. Sakurada T, Katsumata K, Tan-No K, Sakurada S, Kisara K. The capsaicin test in mice for evaluating tachykinin antagonists in the spinal cord. *Neuropharmacology*. 1992; 31:1279-1285.
 26. Koster R, Anderson M, De Beer EJ. Acetic acid for analgesic screening. *Fed Proc*. 1959; 18:412.
 27. Winter CA, Risley EA, Nuss GW. Carrageenan-induced edema in hind paw of the rat as an assay for antiinflammatory drugs. *Proc Soc Exp Biol Med*. 1962; 111:544-552.
 28. Millan MJ, Bervoets K, Rivet JM, Widdowson P, Renouard A, Le Marouille-Girardon S, Gobert A. Multiple $\alpha 2$ -adrenergic receptor subtypes: II. Evidence for a role of rat R and 2A-ARs in the control of nociception, motor behaviour and hippocampal synthesis of noradrenaline. *J Pharmacol Exp Ther*. 1994; 270:958-972.
 29. Chinen CC, Frussa-Filho R. Conditioning to injection procedures and repeated testing increase sch 23390-induced catalepsy in mice. *Neuropsychopharmacology*. 1999; 21:670-678.
 30. Mózsik Gy, Móron F, Jávör T. Cellular mechanisms of the development of gastric mucosal damage and of gastric cytoprotection induced by prostacyclin in rats: A pharmacological study. *Prostaglandins Leukot Med*. 1982; 9:71-84.
 31. Joshi SK, Hernandez G, Mikusa JP, Zhu CZ, Zhong C, Salyers A, Wismer CT, Chandran P, Decker MW, Honore P. Comparison of antinociceptive actions of standard analgesics in attenuating capsaicin and nerve-injury-induced mechanical hypersensitivity. *Neuroscience*. 2006; 143:587-596.
 32. Berkenkopf JW, Weichman BM. Production of prostacyclin in mice following intraperitoneal injection of acetic acid, phenylbenzoquinone and zymosan: its role in the writhing response. *Prostaglandins*. 1988; 36:693-709.
 33. Wantuch C, Piesla M, Leventhal L. Pharmacological validation of a model of cystitis pain in the mouse. *Neurosci Lett*. 2007; 421:250-252.
 34. Stepanovic-Petrovic RM, Tomic MA, Vuckovic SM, Paranos S, Ugresic ND, Prostran MS, Milovanovic S, Boskovic B. The antinociceptive effects of anticonvulsants in a mouse visceral pain model. *Anesth Analg*. 2008; 106:1897-1903.
 35. Tanabe M, Takasu K, Kasuya N, Shimizu S, Honda M, Ono H. Role of descending noradrenergic system and spinal $\alpha 2$ -adrenergic receptors in the effects of gabapentin on thermal and mechanical nociception after partial nerve injury in the mouse. *Br J Pharmacol*. 2005; 144:703-714.
 36. Governo RJ, Morris PG, Marsden CA, Chapman V. Gabapentin evoked changes in functional activity in nociceptive regions in the brain of the anaesthetized rat: an fMRI study. *Br J Pharmacol*. 2008; 153:1558-1567.
 37. Kazi JA, Gee CF. Effect of gabapentin on c-Fos expression in the CNS after paw surgery in rats. *J Mol Neurosci*. 2007; 32:228-234.
 38. Kazi JA, Gee CF. Gabapentin completely attenuated the acute morphine induced c-Fos expression in the rat striatum. *J Mol Neurosci*. 2007; 32:47-52.
 39. Pastoriza LN, Morrow TJ and Casey KL. Medial frontal cortex lesions selectively attenuate the Hot Plate response-possible nocifensive apraxia in the rat. *Pain*. 1996; 64:11-17.
 40. Hendrich J, Van Minh AT, Hebllich F, Nieto-Rostro M, Watschinger K, Striessnig J, Wratten J, Davies A, Dolphin AC. Pharmacological disruption of calcium channel trafficking by the $\alpha 2\delta$ ligand gabapentin. *Proc Natl Acad Sci U S A*. 2008; 105:3628-3633.
 41. Fehrenbacher JC, Taylor CP, Vasko MR. Pregabalin and gabapentin reduce release of substance P and CGRP from rat spinal tissues only after inflammation or activation of protein kinase C. *Pain*. 2003; 105:133-141.
 42. Coderre TJ, Kumar N, Lefebvre CD, Yu JSC. Evidence that gabapentin reduces neuropathic pain by inhibiting the spinal release of glutamate. *J Neurochem*. 2005; 94:1131-1139.
 43. Haraguchi K, Ito K, Kotaki H, Sawada Y, Iga T. Prediction of drug-induced catalepsy based on dopamine

- D1, D2, and muscarinic acetylcholine receptor occupancies. *Drug Met Disp.* 1997; 25:675-684.
44. Olson WL, Gruenthal M, Mueller ME, Olson WH. Gabapentin for parkinsonism: a double-blind, placebo-controlled, crossover trial. *Am J Med.* 1997; 102:60-66.
 45. Van Blercom N, Lasa A, Verger K, Masramón X, Sastre VM, Linazasoro G. Effects of gabapentin on the motor response to levodopa: a double-blind, placebo-controlled, crossover study in patients with complicated Parkinson disease. *Clin Neuropharmacol.* 2004; 27:124-128.
 46. Pfeffer G, Chouinard G, Margolese HC. Gabapentin in the treatment of antipsychotic-induced akathisia in schizophrenia. *Int Clin Psychopharmacol.* 2005; 20:179-181.
 47. Zaccara G, Gangemi PF, Cincotta M. Central nervous system adverse effects of new antiepileptic drugs A meta-analysis of placebo-controlled studies. *Seizure.* 2008; 17:405-421.
 48. Raju PM, Walker RW, Lee MA. Dyskinesia induced by gabapentin in idiopathic Parkinson's disease. *Mov Disord.* 2007; 22:288-289.
 49. Lai MH, Wang TY, Chang CC, Tsai KC, Chang ST. Hemichorea associated with gabapentin therapy with hypoperfusion in contralateral basal ganglion - a case of a paraplegic patient with neuropathic pain. *J Clin Pharm Ther.* 2008; 33:83-86.
 50. Hayashida K, DeGoes S, Curry R, Eisenach JC. Gabapentin activates spinal noradrenergic activity in rats and humans and reduces hypersensitivity after surgery. *Anesthesiology.* 2007; 106:557-562.

(Received December 30, 2008; Accepted January 4, 2009)

Original Article**Enhancement of the dissolution profile of Tenoxicam by a solid dispersion technique and its analytical evaluation using HPLC**Manal K. Darwish^{1,*}, Manal M. Foad²¹ Department of Pharmaceutics, Faculty of Pharmacy (Girls), Al-Azhar University, Cairo, Egypt;² Department of Analytical Chemistry, Faculty of Pharmacy (Girls), Al-Azhar University, Cairo, Egypt.

ABSTRACT: The aim of the present study was to improve the dissolution, and therefore the bioavailability, of poorly water-soluble tenoxicam. Solid dispersions consisting of tenoxicam with two different types of polymers were prepared. The first type were PVP₃₀ and β -cyclodextrin and the second type were two superdisintegrants, explotab and croscarmellose sodium. A solid dispersion with an explotab ratio of 1:1 (F₈) had the best dissolution profile compared to all of the prepared solid dispersions as well as the pure drug, which was then formulated into tablets (T₂F₈). T₂F₈ had far better dissolution than commercial tablets, releasing only 28.3% of the drug, while T₂F₈ exhibited 96.5% drug release in 20 min. T₂F₈ was subjected to analytical validation as well as stability studies. The formulation was found to be stable after storage at 40°C for one month, 40°C and 75% relative humidity (40°C/75% RH) for one month, and 60°C for 15 days; this was confirmed by the absence of degraded product prepared in the laboratory by refluxing the drug with 1 N NaOH for 15 min. Infrared (IR) spectroscopy and differential scanning calorimetry (DSC) were performed on T₂F₈ to identify physicochemical interactions between the drug and carrier, hence its effect on dissolution. A simple and rapid HPLC method was also developed to determine tenoxicam in human plasma and was then used in a pharmacokinetic study. Plasma samples were analyzed on a C₁₈ column with a mobile phase of 0.02 M sodium acetate:acetonitrile:methanol (7:2.5:0.5, v/v/v) and UV detection at 375 nm. The linear range of the plasma concentration was 1-16 μ g/mL with a detection limit of 158 ng/mL. Within-day and between-day precision expressed as the relative standard deviation was less than

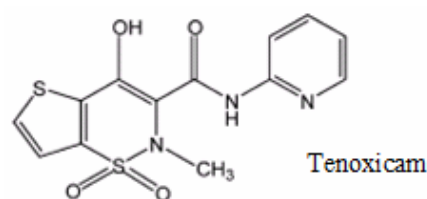
2%. The proposed method was successfully used in a bioequivalence study in healthy volunteers and mean pharmacokinetic parameters were calculated.

Keywords: Tenoxicam, Superdisintegrant, Pharmacokinetic, Solid dispersion, Dissolution enhancement

1. Introduction

Tenoxicam (4-hydroxy-2-methyl-N-(pyridine-2-yl)-2H-thieno-1,2-thiazine-3-carboxamide-1,1-dioxide) (1) is a nonsteroidal anti-inflammatory drug (NSAID) from the oxicam group that also has analgesic and antipyretic properties as a result of inhibiting prostaglandin synthesis (2). Like other oxicam derivatives, tenoxicam has been found to be about 99% protein-bound (3). Due to its accentuated hydrophilic character in comparison to other oxicams, tenoxicam is characterized by less penetration into tissues, explaining its lower incidence of adverse reactions (4). Tenoxicam has recently been studied using IR spectroscopy (5) and spectrophotometric (6-9), chromatographic (10-12), polarographic (13), and pharmacokinetic analysis (14).

Tenoxicam is a poorly water-soluble drug; for such drugs, dissolution plays an important role in their absorption (15). Although it has excellent oral bioavailability, its poor aqueous solubility limits its absorption dissolution rate and thus delays its onset of action. In order to enhance drug solubility in water and in biological fluids, many approaches have recently been devised and include salt formation, solubilization,



*To whom correspondence should be addressed:

Dr. Manal K. Darwish, Pharmaceutics Department, Faculty of Pharmacy (Girls), Al-Azhar University, Cairo, Egypt;
e-mail: maboushady2000@yahoo.com

particle size reduction, solid dispersion (SD), self-dispersing liquid formulations (16), and the use of inclusion compounds based on cyclodextrin (17). Of these methods, solid dispersion is the most efficient. The technique provides a disposition of the drug on the surface of certain materials that can alter the dissolution properties of the drug. Once the solid dispersion is exposed to aqueous media and the carrier is dissolved, the drug is released as very fine colloidal particles (18-20). This results in a greatly enhanced surface area, thus prompting expectations of a high dissolution rate and level of bioavailability for poorly water-soluble drugs (21).

The aim of the present study was to formulate tenoxicam solid dispersions in order to improve dissolution and aqueous solubility to facilitate faster onset of action. Two groups of dissolution enhancers were used in the preparation of solid dispersions, the first group being PVP₃₀ and β -cyclodextrin and the second group being two superdisintegrants, explotab and croscarmellose sodium. Solid dispersions with an improved dissolution profile were characterized using differential scanning calorimetry (DSC) and infra red spectroscopy (IR), and the one with the best dissolution profile was compressed into tablets. A simple and rapid method for the determination of tenoxicam in human plasma as well as in formulated tablets was developed and validated. Linearity range, limits of detection and quantitation, accuracy, precision, and specificity were determined in order to gauge the suitability of the method and confirm results. This method was used successfully in a pharmacokinetic study, revealing bioequivalence between tenoxicam tablets (T₂F₈) and commercial tablets.

2. Materials and Methods

2.1. Materials

Pure tenoxicam (TN) (purity 99.98%), explotab, and croscarmellose sodium (CS) were generously supplied by the Egyptian International Pharmaceutical Company (EIPICO; Tenth of Ramadan City, Egypt). β -Cyclodextrin was obtained from Fluka Chemical Corp., Buchs, Switzerland. Polyvinyl pyrrolidone (PVP K₃₀) was generously supplied by El-Nile Pharmaceutical Co., Cairo, Egypt and Starch 1500 was from Colorcon, Shizuoka, Japan. HPLC-grade acetonitrile and methanol were purchased from Fisher Scientific, Pittsburgh, PA, USA. Sodium acetate and acetic acid were from El-Nasr, Kalubia, Egypt. Tenoxil tablets were obtained commercially.

2.2. Instrumentation

For HPLC, the Agilent-1100 series LC/DAD

(Agilent Technologies, Böblingen, Germany) was used. For spectrophotometry, the Jasco FTIR-5300 spectrophotometer (Jasco Co., Tokyo, Japan) was used. A Shimadzu thermal analyzer (Shimadzu, Kyoto, Japan) was used Along with a United States Pharmacopeia (USP)-standard dissolution apparatus (Model DA-6D) (Veego, Bombay, India). Tableting was done using an EK:O tableting machine (Erweka, Frankfurt, Germany).

2.3. Preparation of tenoxicam physical mixtures and solid dispersions

Solid dispersions of the drug with hydrophilic carriers were prepared in ratios of 1:2, 1:1, and 2:1 of drug:carrier. Two techniques used for preparation were either solvent evaporation or co-grinding. For solvent evaporation, an accurate weighed quantity of tenoxicam was dissolved in a minimum amount of ethanol in which PVP, explotab, and croscarmellose sodium were suspended, the suspension was transferred to a petri dish, the solvent was allowed to evaporate at room temperature for one hour, and the result was then dried in a hot air oven. The mass obtained in each case was crushed, pulverized, and sifted through 80 mesh. For co-grinding, ground mixtures of tenoxicam with β -cyclodextrin were prepared by grinding in a mortar for one minute.

Physical mixtures were formulated for comparison by mixing the drug and carriers in geometric proportions using a spatula without applying pressure. All solid dispersions were stored over anhydrous calcium chloride in a desiccator until further evaluation. The selected formulae are shown in Table 1.

Table 1. Composition of different tenoxicam formulations

Codes	Component	Ratio	Method
PD	Pure drug	–	–
F₁	TN/PVP ₃₀	1:2	SD/Co-evaporation
F₂	TN/PVP ₃₀	1:1	SD/Co-evaporation
F₃	TN/PVP ₃₀	2:1	SD/Co-evaporation
F₄	TN/ β -CD	1:2	SD/Co-grinding
F₅	TN/ β -CD	1:1	SD/Co-grinding
F₆	TN/ β -CD	2:1	SD/Co-grinding
F₇	TN/Explotab	1:2	SD/Co-evaporation
F₈	TN/Explotab	1:1	SD/Co-evaporation
F₉	TN/Explotab	2:1	SD/Co-evaporation
F₁₀	TN/CS	1:2	SD/Co-evaporation
F₁₁	TN/CS	1:1	SD/Co-evaporation
F₁₂	TN/CS	2:1	SD/Co-evaporation
F₁₃	TN/PVP ₃₀	1:2	Physical mixture
F₁₄	TN/PVP ₃₀	1:1	Physical mixture
F₁₅	TN/PVP ₃₀	2:1	Physical mixture
F₁₆	TN/ β -CD	1:2	Physical mixture
F₁₇	TN/ β -CD	1:1	Physical mixture
F₁₈	TN/ β -CD	2:1	Physical mixture
F₁₉	TN/Explotab	1:2	Physical mixture
F₂₀	TN/Explotab	1:1	Physical mixture
F₂₁	TN/Explotab	2:1	Physical mixture
F₂₂	TN/CS	1:2	Physical mixture
F₂₃	TN/CS	1:1	Physical mixture
F₂₄	TN/CS	2:1	Physical mixture

2.4. Characterization of solid dispersions

Solid dispersions were characterized by Fourier transform infrared (FTIR) spectroscopy; the scanning range was 400 to 4,000 cm^{-1} with a resolution of 2 cm^{-1} and differential scanning calorimetry (DSC) was performed at a rate of 5°C per min over the range of 30-300.

2.5. *In vitro* dissolution studies

Dissolution rate studies were performed in 900 mL of 0.1 N HCl (pH 1.2) at $37 \pm 0.5^\circ\text{C}$, using a dissolution apparatus with paddles rotating at 50 rpm. Solid products, solid dispersions of the drug and carriers, and their physical mixtures containing 20 mg tenoxicam were subjected to dissolution; these results were then compared to those for the pure drug. At fixed time intervals, samples were withdrawn, filtered, and spectrophotometrically assayed for drug content at 375 nm. Dissolution efficiency (DE) was calculated from the area under the dissolution curve at time t and expressed as percentage of the area of the rectangle described by 100% dissolution in the same time (22).

2.6. Tablet preparation

Solid dispersions containing tenoxicam with explotab (1:1), croscarmellose sodium (1:2), and PVP₃₀ (2:1) had the maximum *in vitro* dissolution of all prepared formulations, and this is why they were mixed with talc (2%), sodium lauryl sulphate (1%), and magnesium stearate (1%) and then compressed into tablets. The average weight of the tablets was adjusted to 250 mg using Avicel 102, and tablets were coded T₁F₃, T₁F₈, and T₁F₁₀ for tenoxicam/PVP₃₀, tenoxicam/explotab, and tenoxicam/CS, respectively, as shown in Table 2. Starch 1500 was added to the aforementioned formulations as a disintegrating agent and the result was compressed into tablets (T₂F₃, T₂F₈ and T₂F₁₀ in Table 2) to determine whether the presence or absence of a disintegrant would affect the dissolution of the prepared tablets. All ingredients were mixed and compressed in a tableting machine using flat-tip punches and dies with an 8-mm diameter *via* a direct compression technique. *In vitro* dissolution studies for the prepared tablets and commercial tablets were conducted using 900 mL 0.1 N HCl as a dissolution medium at 50 rpm.

Table 2. Composition of tenoxicam tablets

Tablets code	Component	Starch 1500
T ₁ F ₃	TN/PVP ₃₀	–
T ₁ F ₈	TN/Explotab	–
T ₁ F ₁₀	TN/CS	–
T ₂ F ₃	TN/PVP ₃₀	5%
T ₂ F ₈	TN/Explotab	5%
T ₂ F ₁₀	TN/CS	5%

2.7. Stability study of tablet

In order to determine any changes in the *in vitro* drug release profile as a result of storage, a stability study of T₂F₈ tablets containing tenoxicam/explotab, which had the maximum dissolution release, was conducted at 40°C for one month, 40°C and 75% relative humidity (40°C/75% RH) for one month, and 60°C for 15 days.

2.8. Validation of the HPLC method

Tenoxicam was subjected to analytical validation in human plasma using an HPLC method according to USP guidelines, from which the recovery of the prepared T₂F₈ can be calculated.

2.8.1. Preparation of standard solutions

Different aliquots (0.01-0.16 mg) of the standard tenoxicam in methanol, 0.1 mg/mL were introduced into a series of 10-mL volumetric flasks and adjusted to volume with methanol. One mL of each solution was transferred to a series of 5-mL centrifuge tubes, each containing 1 mL blank plasma. Zero point three mL of acetonitrile/perchloric acid mixture (2:1) were added to each tube, vortexed for 30 sec, and then centrifuged at 5,000 rpm for 10 min.

2.8.2. Linearity

The linearity of the method was evaluated using a calibration curve in the range of 1-16 $\mu\text{g/mL}$ tenoxicam. Twenty μL injections were made in triplicate for each concentration and chromatographed on a C₁₈ column at ambient temperature using a mobile phase of 0.02 M sodium acetate (pH 2.7)-acetonitrile-methanol (70:25:5, v/v/v) at a flow rate of 1 mL/min and UV detection at 375 nm. The calibration curve was obtained by plotting the peak area as a function of drug concentration and the regression parameters were determined.

2.8.3. Accuracy and precision

The intraday and interday accuracy and precision were determined by replicate analysis of three sets of samples spiked with three different concentrations of tenoxicam (2, 8, and 16 $\mu\text{g/mL}$) within one day or on three consecutive days.

2.8.4. Recovery

Absolute recovery of tenoxicam was determined in triplicate by extracting blank human plasma samples spiked with tenoxicam; the mean peak area was compared to that obtained from the standard drug with the same concentration.

2.8.5. Specificity

The proposed method successfully quantitated tenoxicam even in the presence of degradation products. Forced degradation of the pure drug was performed in the laboratory where 10 mg of tenoxicam were transferred to a 100-mL conical flask. Twenty mL of 1 M NaOH were added and refluxed for 20 min. After cooling, 5 M HCl was added to the drug solution until the pH was adjusted to 8. The solution was then evaporated under a vacuum, extracted three times with 20 mL methanol, filtered into a 100-mL volumetric flask, and brought to volume with methanol. The obtained solution was labeled as contain degradates derived from 0.1 mg/mL tenoxicam. Laboratory-prepared mixtures containing different ratios of pure and degraded drug were analyzed using the proposed HPLC method.

2.8.6. Analysis of tenoxicam in T_2F_8 tablets

Ten prepared T_2F_8 tablets were weighed, finely ground, and mixed. The amount of fine powder equivalent to 10 mg tenoxicam was sonicated with 70 mL methanol for 15 min, filtered into a 100-mL volumetric flask, and brought to volume with methanol. The obtained solution was labeled as containing 0.1 mg/mL and analyzed after spiking by the proposed HPLC method, as described previously in the section on linearity.

2.9. Bioavailability study

The selected tablet formula T_2F_8 with the maximum dissolution profile (with a tenoxicam/explotab ratio of 1:1) and commercial tablets were subjected to a single-dose relative pharmacokinetic study. The study was a crossover bioavailability design that was performed using 6 healthy adult male volunteers between the ages of 22 and 30 years and weighing between 60 and 85 kg. The volunteers were prevented from taking any alcohol or drugs for 2 days prior to experiment and during the study. The volunteers fasted for 8 h before drug administration. Each subject ingested 2 compressed tablets of the two products (test and reference). An interval of 14 days was allowed prior to the next treatment. Whole blood samples were taken from a forearm vein pre-dose and at 1, 2, 3, 4, 5, 6, and 8 h post-dosing. The blood was centrifuged at 5,000 rpm for 10 min, and the plasma obtained was stored at -20°C until analysis. To compare the rate and extent of absorption of tenoxicam, the following pharmacokinetic variables were calculated for each volunteer using actual blood sampling times. The maximum plasma concentration (C_{max}) and the time required to reach this concentration (T_{max}) were read directly from the arithmetic plot of time vs. plasma concentration for tenoxicam. The overall elimination

rate constant (k_e) was calculated from the slope of the terminal elimination phase of a semilogarithmic plot of concentration vs. time after subjecting it to linear regression analysis. The elimination half-life ($t_{1/2}$) was obtained by dividing 0.693 by k_e . The absorption rate constant (k_a) was calculated using the method of residuals (23). The area under the plasma tenoxicam concentration vs. time curve ($\text{AUC}_{0-\infty}$) was determined by means of the trapezoidal rule. The relative bioavailability of tenoxicam from matrix tablets in comparison to a reference formulation (commercial tablets) was calculated by dividing its $\text{AUC}_{0-\infty}$ by that of the commercial tablet dosage form.

3. Results and Discussion

3.1. Characterization of solid dispersions

3.1.1. Differential scanning calorimetry

Thermograms were carried out separately with the drug and carriers as shown in Figure 1. The DSC curve for tenoxicam had one endothermic peak at about 225°C , corresponding to its melting point, while crospovidone, explotab, and PVP had broad peaks at 80.8 , 78.4 , and 72.7°C , respectively. On the other hand, thermograms for all physical mixtures indicate that there was no appreciable shift in the melting peak of tenoxicam with all carriers. This was also true for

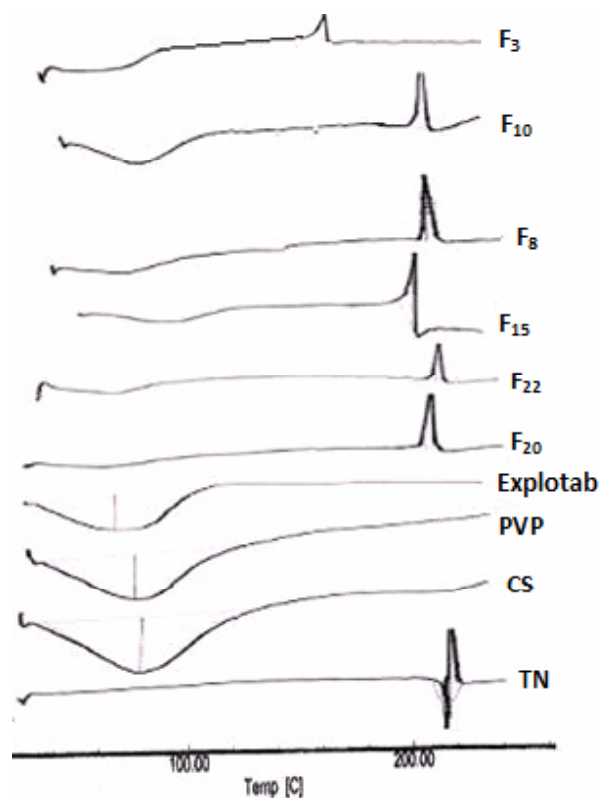


Figure 1. DSC thermogram of tenoxicam, carriers, their physical mixtures, and corresponding solid dispersions.

solid dispersions of the drug with croscarmellose and explotab, indicating the absence of strong interactions between the components. The increase in the dissolution rate was thus attributed to an increase in the available surface area of the drug due to improved wettability provided by the superdisintegrants. In the case of drug/PVP solid dispersion, the peak shifted slightly to a lower temperature (203°C); this may be due to a low carrier ratio in the solid dispersion, but a notable decrease in peak intensity is evidence of its formation.

3.1.2. Fourier transform infrared (FTIR) spectroscopy

Figure 2 shows the IR spectra for tenoxicam in physical mixtures and solid dispersions with different carriers. The IR spectrum of the plain drug had an absorption band at $3,395\text{ cm}^{-1}$ due to an O–H stretching vibration; the broadness of this band is indicative of hydrogen bonding. The strong band observed at $1,636\text{ cm}^{-1}$ is attributed to the carbonyl stretching vibration in the secondary amide group (CO–NH). The band located at $1,597\text{ cm}^{-1}$ is due to the stretching vibration of pyridyl nitrogen (C=N). Addition of the carriers studied to pure tenoxicam resulted in no shifting for any of these characteristic bands, indicating no chemical interaction between the drug and the polymers used.

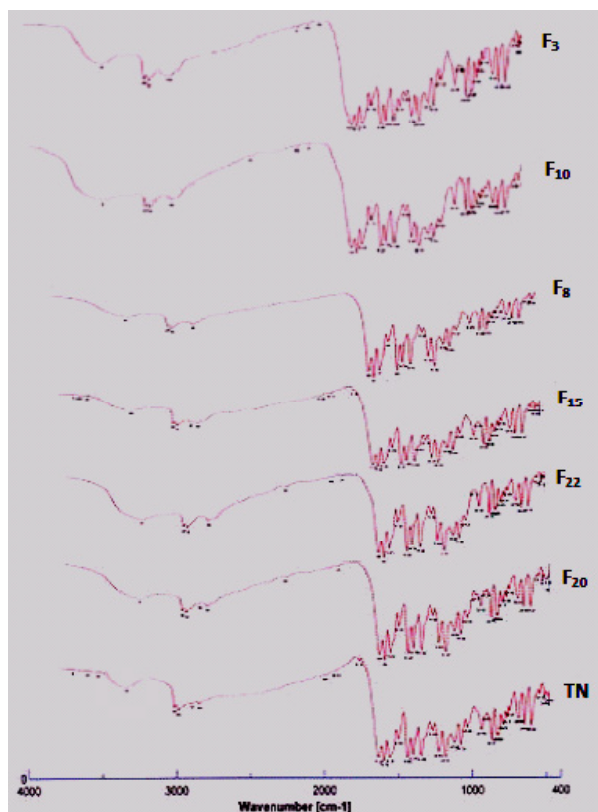


Figure 2. IR spectra of tenoxicam, physical mixtures, and corresponding solid dispersions for the chosen formulations.

3.2. In vitro dissolution studies

Dissolution profiles of the pure drug and drug-carrier binary systems are represented in Figures 3-6. As is apparent, the solid dispersion technique improved the dissolution rate of tenoxicam to a great extent. This is clearly evident from the % of drug dissolved in 20 min (DP_{20}) and dissolution efficiency at 60 min (DE_{60}) for

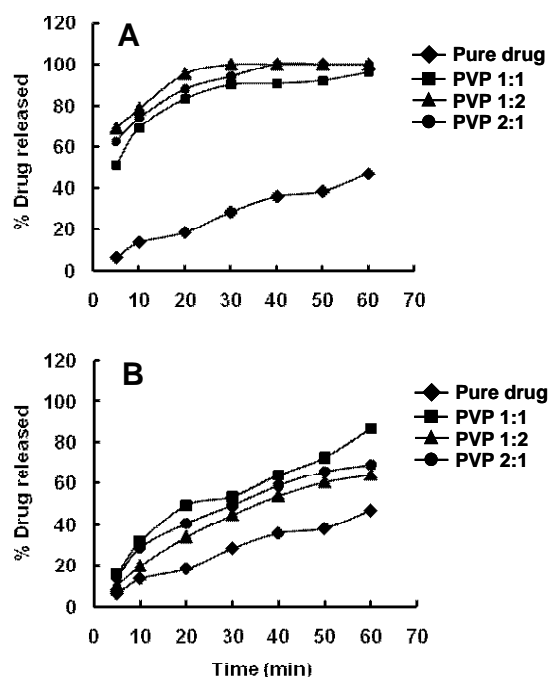


Figure 3. % drug released from solid dispersions (A) and physical mixtures (B) prepared with PVP_{30} in different ratios.

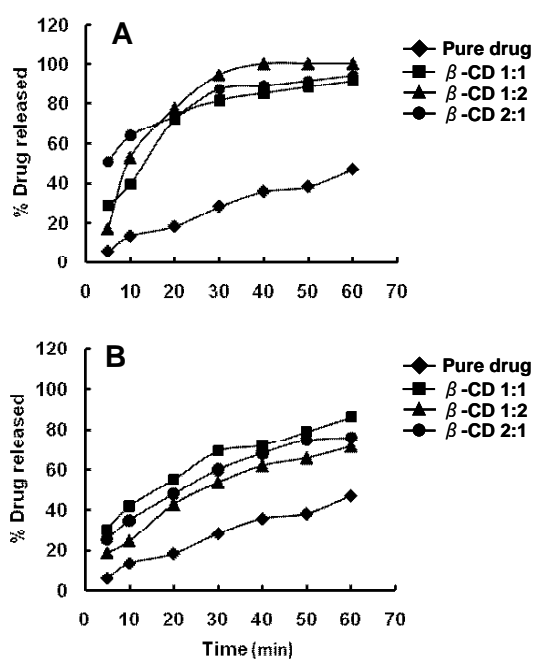


Figure 4. % drug released from solid dispersions (A) and physical mixtures (B) prepared with β -CD in different ratios.

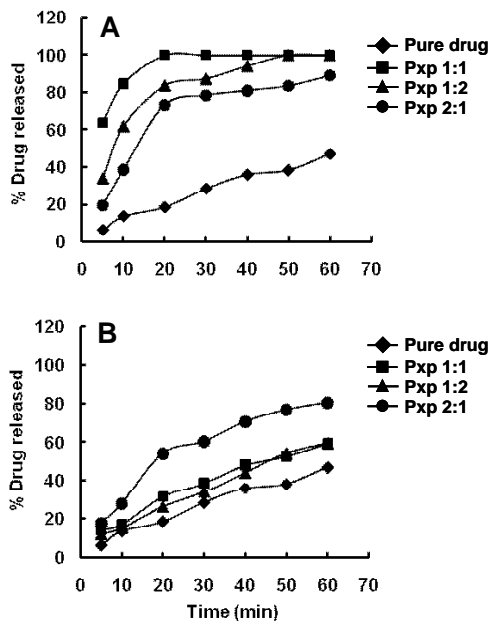


Figure 5. % drug released from solid dispersions (A) and physical mixtures (B) prepared with explotab in different ratios.

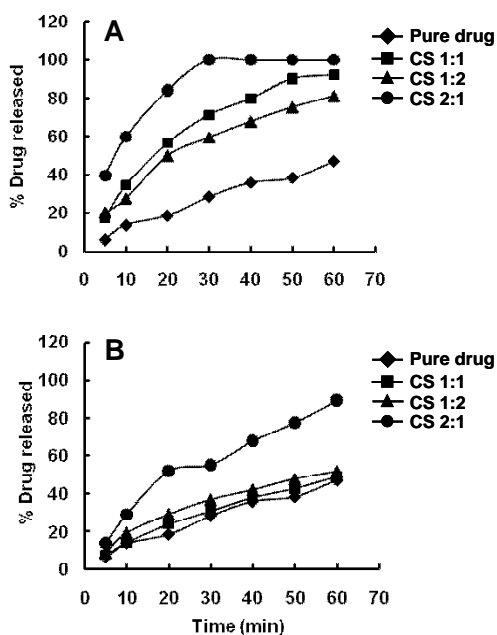


Figure 6. % drug released from solid dispersions (A) and physical mixtures (B) prepared with croscarmellose in different ratios.

the pure drug and its binary systems with carriers, as presented in Table 3. Solid dispersions formulated with a drug/PVP ratio of 2:1 had a DP_{20} and DE_{60} of 95.4% and 91.1%, respectively, in comparison to 18.5% for pure drug powder. Decreased crystallinity and increased wetting of the particles may be considered major contributors to the enhanced dissolution of tenoxicam from a solid dispersion system containing PVP (24). Solid dispersions with β -cyclodextrin as a carrier had an increase in drug release in comparison to the pure

Table 3. Dissolution parameters for different tenoxicam formulations

SSD codes	Component	Ratio	DP_{20} (%) [*]	DE_{60} (%) ^{**}
PD	Pure drug	–	18.5 ± 1.04	29.67
F ₁	TN/PVP ₃₀	1:2	88.0 ± 3.50	88.80
F ₂	TN/PVP ₃₀	1:1	83.2 ± 0.45	82.16
F ₃	TN/PVP ₃₀	2:1	95.4 ± 2.06	91.10
F ₄	TN/ β -CD	1:2	73.9 ± 1.34	79.90
F ₅	TN/ β -CD	1:1	72.3 ± 1.67	73.26
F ₆	TN/ β -CD	2:1	77.7 ± 1.55	82.49
F ₇	TN/Explotab	1:2	73.3 ± 3.09	69.70
F ₈	TN/Explotab	1:1	99.8 ± 2.44	91.52
F ₉	TN/Explotab	2:1	83.7 ± 2.98	82.95
F ₁₀	TN/CS	1:2	84.3 ± 2.76	86.15
F ₁₁	TN/CS	1:1	56.7 ± 2.44	68.60
F ₁₂	TN/CS	2:1	49.9 ± 1.34	58.70
F ₁₃	TN/PVP ₃₀	1:2	40.8 ± 1.32	50.68
F ₁₄	TN/PVP ₃₀	1:1	49.4 ± 1.98	57.18
F ₁₅	TN/PVP ₃₀	2:1	34.0 ± 1.22	45.39
F ₁₆	TN/ β -CD	1:2	47.9 ± 1.55	58.84
F ₁₇	TN/ β -CD	1:1	55.0 ± 2.49	64.72
F ₁₈	TN/ β -CD	2:1	42.7 ± 1.27	54.06
F ₁₉	TN/Explotab	1:2	54.2 ± 3.22	59.77
F ₂₀	TN/Explotab	1:1	31.4 ± 1.87	40.61
F ₂₁	TN/Explotab	2:1	26.3 ± 1.54	38.89
F ₂₂	TN/CS	1:2	51.9 ± 1.76	59.49
F ₂₃	TN/CS	1:1	24.1 ± 1.23	32.43
F ₂₄	TN/CS	2:1	29.3 ± 2.55	36.53

^{*} DP_{20} : Percent drug dissolved in 20 min. ^{**} DE_{60} : Dissolution efficiency at $t = 60$ min. (calculated from the area under the dissolution curve at $t = 60$ min and expressed as a % of the area of the rectangle described by 100% dissolution in the same time). Each value is the average of three determinations.

drug, as shown in Figure 4. Table 3 represents DP_{20} and DE_{60} of 77.7% and 82.49%, respectively, for TN/ β -CD (2:1-SD). This enhancement can be attributed to the greater hydrophilic character of the systems due to the presence of the carrier, which can reduce interfacial tension between a poorly water-soluble drug and dissolution medium (25).

Moreover, in the case of β -cyclodextrin the carrier dissolves more rapidly than the drug in the early stage of the dissolution process. Hence, it can act on the hydrodynamic layer surrounding the drug particles, resulting in an *in situ* inclusion process that improves the dissolution of the drug. In fact, systems containing a larger amount of β -cyclodextrin had faster drug dissolution. The addition of the two superdisintegrants markedly improved the dissolution rate of the formulated solid dispersions in comparison to the pure drug; even their physical mixtures displayed an increase in drug release, as shown in Table 3 and Figures 5 and 6. Formulations prepared with explotab had a great increase in dissolution behavior as noted from DP_{20} values; a formulation with a 1:1 ratio had the highest DP_{20} value (99.80%) and a DE_{60} of 91.52%. Explotab was expected to absorb a large amount of water when exposed to dissolution medium and swell, thus resulting in the wetting of small drug particulates deposited on the surface of explotab. The carrier swelling would cause deaggregation of clusters of small drug particles and facilitate their dissolution. The improved dissolution in formulations with croscarmellose (Figure 6) could also be due to a reduction in the particle size of

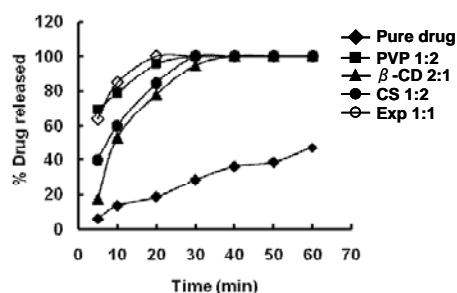


Figure 7. % drug released from solid dispersions exhibiting maximum release in comparison to the pure drug.

Table 4. Dissolution parameters for tenoxicam tablets

Tablets code	DP ₂₀ (%) [*]	DE ₆₀ (%) ^{**}
Commercial	28.3	42.82
T ₁ F ₃	32.8	49.59
T ₁ F ₈	86.8	84.53
T ₁ F ₁₀	63.0	72.65
T ₂ F ₃	53.4	74.23
T ₂ F ₈	96.5	93.77
T ₂ F ₁₀	86.6	86.70

^{*} DP₂₀: Percent drug dissolved in 20 min. ^{**} DE₆₀: Dissolution efficiency at $t = 60$ min. (calculated from the area under the dissolution curve at $t = 60$ min and expressed as a % of the area of the rectangle described by 100% dissolution in the same time). Each value is the average of three determinations.

the drug, its deposition on the surface of the carrier, and improved hydrophilicity. Figure 7 shows the superior drug release rate for each carrier used. A PVP₃₀ ratio of 1:2, a β -CD ratio of 2:1, an explotab ratio of 1:1, and a croscarmellose ratio of 1:2 resulted in maximum drug release in comparison to other formulations as well as the pure drug.

3.3. *In vitro* dissolution studies for tablets

Based on *in vitro* dissolution performance, solid dispersions with a PVP₃₀ ratio of 2:1, explotab ratio of 1:1, and croscarmellose ratio of 1:2 were selected for compression into tablets since they had superior drug release rates. Table 4 shows a comparison of the percent drug released in 20 min (DP₂₀) as well as dissolution efficiency at 60 min (DE₆₀) in tablets prepared from the selected solid dispersions with different carriers and that of commercial tablets. As is apparent from the table, T₂F₃, T₂F₈, and T₂F₁₀ had a DP₂₀ of 53.4, 96.5, and 86.6%, respectively, while they had a DE₆₀ of 74.23, 93.77, and 86.7%, respectively. They also had a higher drug release than tablets without disintegrant (T₁F₃, T₁F₈, and T₁F₁₀) in which the disintegration step was not enhanced. Figure 8 shows a delay in the release of the drug from tablets in comparison to their solid dispersions due to the time taken (several minutes) by the disintegration step in tablets.

3.4. Stability study of tablets

In order to determine any changes in the *in vitro* drug

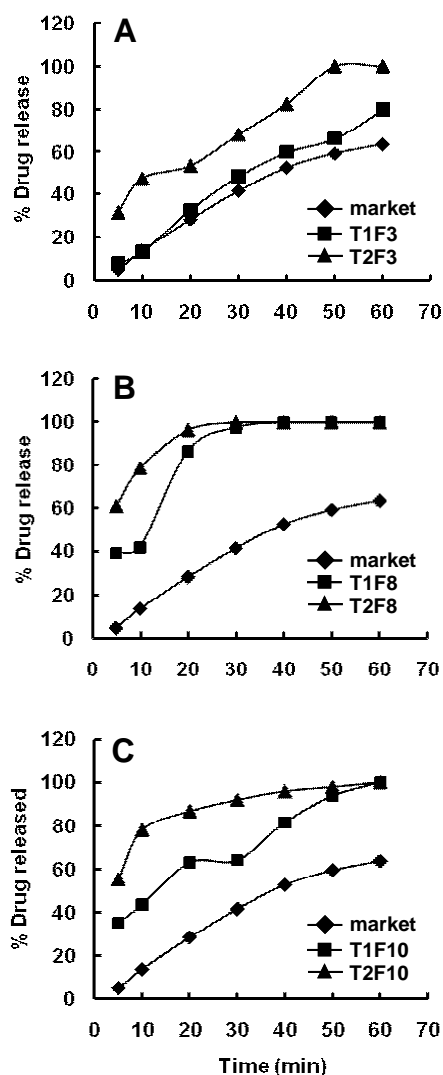
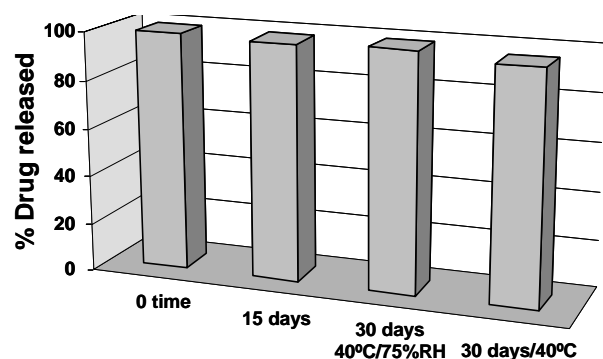


Figure 8. % drug released from commercial tablets and formulated tablets with and without disintegrant, for tablets prepared with PVP₃₀ (A), tablets prepared with Explotab (B) and tablets prepared with croscarmellose (C) in comparison to commercial tablets.

release profile as a result of storage, a stability study of tablets containing tenoxicam/explotab, which had the maximum dissolution release, was conducted at 40°C for one month, 40°C and 75% relative humidity (40°C/75%RH) for one month, and 60°C for 15 days. As shown in Figure 9, under these conditions no significant changes in the tenoxicam release profile from T₂F₈ tablets were observed. This similarity in drug release was confirmed by data obtained from values for the difference factor (f_1), and similarity factor (f_2). These factors help to assure similarity in product performance according to the US Food and Drug Administration's guides for industry (26). Generally f_1 values up to 15 (0-15) and f_2 values greater than 50 (50-100) ensure sameness or equivalence of the two curves (27,28). Table 5 shows values for f_1 and f_2 obtained from *in vitro* dissolution data for tenoxicam-explotab tablets after storage for the aforementioned times. All values were within the accepted range, indicating the similarity of all tablets at all storage times.

Table 5. Results of similarity factors obtained after different storage times

Factors	T ₂ F ₈ (15 days)	T ₂ F ₈ (30 days) (40°C/75% RH)	T ₂ F ₈ (30 days) (40°C)
f ₁	3	8	10
f ₂	71	68	64

**Figure 9.** % drug release of (T₂F₈) tablet after different storage times.

3.5. Validation data

3.5.1. Optimization of chromatographic conditions

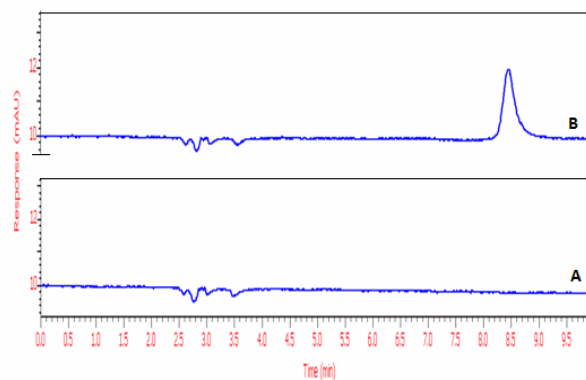
Different chromatographic conditions affecting the separation process were studied and optimized. Different compositions of the mobile phase, flow rates, and wavelengths were tried. Tenoxicam's peak was resolved by using a reversed-phase Nucleosil C₁₈ column (particle size: 5 μm, 250 mm × 4.6 mm), a mobile phase of 0.02 M sodium acetate (pH 2.7) acetonitrile-methanol (70:25:5, v/v/v) at a flow rate of 1 mL/min, and UV detection at 375 nm. Under these conditions, the drug exhibited a sharply resolved peak at 8.2 min. A chromatogram of human blank plasma and blank plasma spiked with tenoxicam is shown in Figure 10.

3.5.2. Linearity

According to peak area-response at 375 nm, Beer's law was obeyed over the range of 1-16 μg/mL of tenoxicam, with a high correlation coefficient (0.9998). The limit of quantitation (LOD) was assessed using the slope of calibration curve and standard deviation of the blank and was found to be 526 ng/mL, as shown in Table 6.

3.5.3. Accuracy and precision

Inter- and intraday accuracy and precision of the proposed procedure were calculated. Inter- and intraday accuracy (expressed as R%) ranged from 97.1 to 98.3 and from 98.5 to 98.9, respectively. However, precision (expressed as RSD%) ranged from 0.21 to 0.95 and from 0.84 to 1.32, respectively, as shown in Table 6.

**Figure 10.** Chromatogram of human blank plasma (A) and blank plasma spiked with tenoxicam (B).**Table 6.** Selected spectral data for the determination of spiked tenoxicam by the proposed HPLC procedure

Parameter	HPLC procedure
Linearity range (μg/mL)	1-16
λ _{max}	375 nm
LOD (ng/mL)	158
LOQ (ng/mL)	526
Regression parameters	
Slope ± SD (S _b)	9,842 ± 33.9
Intercept ± SD (S _a)	-108.6 ± 279.9
SD of residual (S _{xy})	413.6
Correlation coefficient (r ²)	0.9998
Accuracy (R%)	
Interday	97.1 - 98.3
Intraday	98.5 - 98.9
Precision (RSD%)*	
Interday	0.21 - 0.95
Intraday	0.84 - 1.32

* n = 9.

Table 7. Absolute recovery of tenoxicam from spiked human plasma

Taken conc. (μg/mL)	Found conc. (μg/mL)	Recovery (%)
2	1.73	86.5
6	5.29	88.2
10	8.66	86.6
14	12.21	87.2
16	13.83	86.4
Mean ± SD%	-	86.98 ± 0.75

3.5.4. Absolute recovery

Using the proposed HPLC method, absolute recovery of the drug ± SD was 86.98 ± 0.75% (Table 7).

3.5.5. Specificity

The pure drug was selectively determined using the proposed HPLC method in the presence of up to 95% of its alkaline induced degradation product with a mean recovery of 99.92 ± 1.01%. Peaks at 2.4 and 3.4 min for degradates were well resolved from the intact tenoxicam peak at 8.2 min (Figure 11). A suggested degradation pathway was proposed (Scheme 1) and verified by the IR spectra of both the drug and degradates.

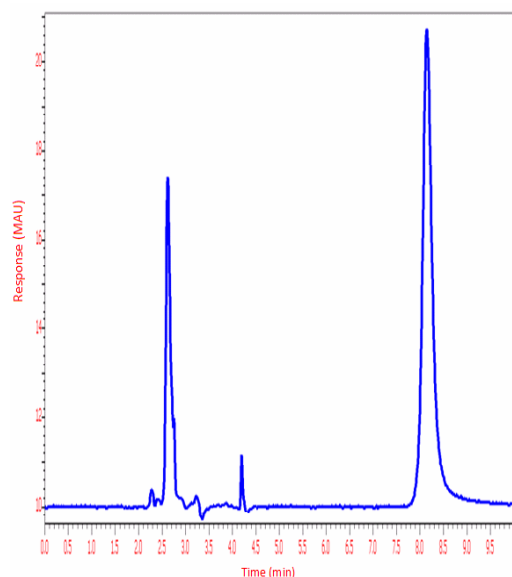
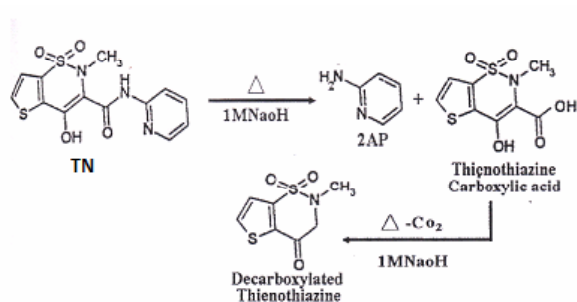


Figure 11. HPLC chromatogram of a mixture of tenoxicam and its degradates.



Scheme 1. Degradation pathway of tenoxicam.

Table 8. Statistical analysis of the results obtained by the proposed procedure for the determination of tenoxicam in the prepared T₂F₈ tablets in comparison to those from a conventional method

Parameter	Proposed HPLC procedure	Conventional method (6)
<i>n</i>	5	6
Mean recovery%	97.23	99.3
<i>SD</i>	0.69	0.51
Variance	0.47	0.26
<i>t</i> [*]	0.552 (2.262)	—
<i>F</i> [*]	1.83 (5.19)	—

* Values in parentheses are the theoretical *t* and *F* values at *P* = 0.05.

Appearance of a single peak at 8.3 min in the chromatogram of the prepared T₂F₈ tablets proved the successful evaluation of tenoxicam in the prepared tablets without interference from additives with a mean recovery of 97.23 ± 0.69%. This was then compared statistically to the results of a conventional method (6); no significant differences were found between the two methods at a probability of 95% (Table 8).

3.6. Bioavailability studies

The mean tenoxicam plasma concentration vs. time profiles is shown in Figure 12. The mean

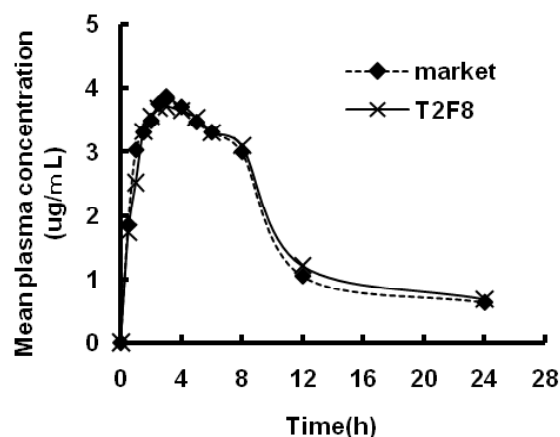


Figure 12. Mean plasma concentration of tenoxicam after oral administration of T₂F₈ tablets in comparison to commercial tablets.

Table 9. Mean pharmacokinetic parameters for tenoxicam after oral administration of T₂F₈ tablets in human volunteers

Pharmacokinetic parameters	Volunteers orally administered	
	T ₂ F ₈ tablets	Commercial tablets
AUC (0-24)	25.62	26.05
AUC _{0-∞} (μg/mL/h)	90.71	83.56
<i>t</i> _{1/2} (h)	0.653782	0.867316
<i>k</i> _a (h ⁻¹)	1.059986	0.799017
<i>T</i> _{max} (h)	2.5	3.0
<i>C</i> _{max} (μg/mL)	3.72	3.87
Relative bioavailability (%)	108.54	—

pharmacokinetic parameters calculated from individual plasma tenoxicam concentrations vs. time profiles are summarized in Table 9.

Mean values for the two preparations were close together. Based on statistical data, pharmacokinetic parameters of the two preparations indicated bioequivalence. The relative bioavailability of tenoxicam tablet was found to be 108.54 %.

4. Conclusion

Based on the current study, improvement in the dissolution of the water-insoluble drug tenoxicam was achieved through solid dispersion using different carriers, the best of which was explotab, which exhibited complete drug release in 20 min. A tenoxicam/explotab solid dispersion was then compressed into tablets but its enhanced dissolution profile was maintained. Moreover, a sensitive and rapid method was provided for the analysis of tenoxicam in human plasma either in bulk or in pharmaceutical formulations. Validation of the proposed method was carried out according to USP guidelines; results were precise and accurate. The short duration of the assay and its specificity allowed for the use of the method in routine analysis and in a pharmacokinetic study, where the formulated tablet was found to be bioequivalent to commercial tablets when taken by human volunteers.

Acknowledgments

The authors would like to thank the International Pharmaceutical Company (EIPICO), Egypt, for their donation of tenoxicam.

References

1. British Pharmacopoeia Commission. British pharmacopoeia. 2008; vol. II, Crown copyright. 2007; pp. 2089-2090.
2. Hye SG, In KC. Effect of vehicles and penetration enhancers on the *in vitro* percutaneous absorption of tenoxicam through hairless mouse skin. *Int J Pharm.* 2002; 236:57-64.
3. Sora L, Toma G, Stefan U, Jean N, Victor D, Andrei M. Fast RPLC-UV method on short sub-two microns particles packed column for the assay of tenoxicam in plasma samples. *J Pharm and Biom Anal.* 2007; 43:1437-1443.
4. Nilson OG. Clinical pharmacokinetics of tenoxicam. *Clin Pharmacokinet.* 1994; 26:16-43.
5. Atay O, Dincol F. Quantitative determination of tenoxicam by infra-red spectrophotometry. *Anal LeH.* 1997; 30:1675-1684.
6. El-Walily AFM, Blaih SM, Barary MH, El Sayed MA, Abdine HH, El-Kersh AM. Simultaneous determination of tenoxicam and 2-aminopyridine using derivative spectrophotometry. *J pharm Biomrd Anal.* 1997; 15:1923-1928.
7. El-Ries MA. Spectrophotometric determination of piroxicam and tenoxicam in pharmaceutical preparations using uranyl acetate as a chromogenic agent. *Anal LeH.* 1998; 31:793-807.
8. Vi jayaraghavan C, Vi jayaraj R. Spectrophotometric determination of tenoxicam in plasma and urine samples. *Indian-Drugs.* 1997; 34:604-605.
9. Amin AS. Spectrophotometric determination of tenoxicam in pharmaceutical formulation using alizarin. *J Pharm Biomed Anal.* 2002; 29:729-736.
10. Taha EA, Salama NN, Fattah LE. Stability indicating chromatographic methods for the determination of some oxicams. *J AOAC-Int.* 2004; 87:366-373.
11. Joseph J, Bertucat M. Selective assays for quantitation of tenoxicam in presence of its photodegradation products. *J Liq Chromatogr Relat Technol.* 1999; 22:2009-2021.
12. Mason JL, Hobbs GJ. Simple method for the analysis of tenoxicam in human plasma using high performance liquid chromatography. *J Chromatogr B Biomed Appl.* 1995; 665:410-415.
13. Atkopar Z, Tuncel M. The polarographic determination of tenoxicam in pharmaceutical preparations. *Anal Lett.* 1996; 29:2383-2397.
14. Gao LQ, Wu D, Tao XL, Gang YY. Study on the relative bioavailability of tenoxicam capsules. *Yaowu Fenxi Zazhi.* 2006; 26:589-591.
15. Amidon GL, Lennemas H, Shah VP, Crison JR. A theoretical basis for a biopharmaceutic drug classification: the correlation of *in vitro* drug product dissolution and *in vivo* bioavailability. *Pharm Res.* 2005; 12:413-420.
16. Gershanik T, Benita S. Self dispersing liquid formulations for improving oral absorption of lipophilic drugs. *Eur J pharm.* 2000; 50:179-188.
17. Dixit RP, Nagaresenker MS. *In vitro* and *in vivo* advantage of celecoxib surface solid dispersion and dosage form development. *Ind J Pharm Sci.* 2007; 69:370-377.
18. Vippagunta SR, Maul KA, Tallavajhala S, Grant DJW. Solid-state characterization of nifedipine solid dispersions. *Int J Pharm.* 2002; 236:111-123.
19. Devi VK, Vijayalakhmi P, Avinash M. Preformulation studies on celecoxib with a view to improve bioavailability. *Indian J Pharm Sci.* 2003; 65:542-545.
20. Zedong D, Ashish C, Harpreet S, Duk SC, Hitesh C, Navnit S. Evaluation of solid state properties of solid dispersions prepared by hot-melt extrusion and solvent co-precipitation. *Int J Pharm.* 2008; 355:141-149.
21. Goldberg AH, Galbaldi M, Kanig KL. Increasing dissolution rates and gastrointestinal absorption of drugs *via* solid solutions and eutectic mixtures III. Experimental evaluation of griseofulvin-succinic acid solution. *J Pharm Sci.* 1966; 55:487-492.
22. Khan KA. The concept of dissolution efficiency. *J Pharm Pharmacol.* 1975; 27:48-49.
23. Gibaldi M, Perrier D. *Pharmacokinetics.* New York, NY: Marcel Dekker; 1990.
24. Sethia S, Squillante E. Solid dispersion of carbamazepine in PVP K30 by conventional solvent evaporation and supercritical methods. *Int J Pharm.* 2004; 272:1-10.
25. Mura P, Faucci MT, Parrini PL. Effects of grinding with microcrystalline cellulose and cyclodextrins on the ketofen physicochemical properties. *Drug Dev Ind Pharm.* 2001; 27:119-128.
26. Costa P. An alternative method to the evaluation of similarity factors in dissolution testing. *Int J pharm.* 2001; 220:77-83.
27. FDA. Guidance for industry: Immediate release of oral solid dosage forms—Scale up and post approval changes: chemistry, manufacture, controls, *in vitro* dissolution testing, and *in vivo* bioequivalence documentation. Centre of Drug Evaluation and Research, Rockville, MD, USA, 1995.
28. Shah VP, Tsong Y, Sathe P, Liu JP. *In vitro* dissolution profile comparison--statistics and analysis of the similarity factor, f_2 . *Pharm Res.* 1998; 15:889-896.

(Received January 6, 2009; Accepted January 12, 2009)

Drug Discoveries & Therapeutics

Guide for Authors

1. Scope of Articles

Drug Discoveries & Therapeutics mainly publishes articles related to basic and clinical pharmaceutical research such as pharmaceutical and therapeutical chemistry, pharmacology, pharmacy, pharmacokinetics, industrial pharmacy, pharmaceutical manufacturing, pharmaceutical technology, drug delivery, toxicology, and traditional herb medicine. Studies on drug-related fields such as biology, biochemistry, physiology, microbiology, and immunology are also within the scope of this journal.

2. Submission Types

Original Articles should be reports new, significant, innovative, and original findings. An Article should contain the following sections: Title page, Abstract, Introduction, Materials and Methods, Results, Discussion, Acknowledgments, References, Figure legends, and Tables. There are no specific length restrictions for the overall manuscript or individual sections. However, we expect authors to present and discuss their findings concisely.

Brief Reports should be short and clear reports on new original findings and not exceed 4000 words with no more than two display items. *Drug Discoveries & Therapeutics* encourages younger researchers and doctors to report their research findings. Case reports are included in this category. A Brief Report contains the same sections as an Original Article, but Results and Discussion sections must be combined.

Reviews should include educational overviews for general researchers and doctors, and review articles for more specialized readers.

Policy Forum presents issues in science policy, including public health, the medical care system, and social science. Policy Forum essays should not exceed 2,000 words.

News articles should not exceed 500 words including one display item. These articles should function as an international news source with regard to topics in the life and social sciences and medicine. Submissions are not restricted to journal staff - anyone can submit news articles on subjects that would be of interest to *Drug Discoveries & Therapeutics*' readers.

Letters discuss material published in *Drug Discoveries & Therapeutics* in the last 6 months or issues of general interest. Letters should not exceed 800 words and 6 references.

3. Manuscript Preparation

Preparation of text. Manuscripts should be written in correct American English and submitted as a Microsoft Word (.doc) file in a single-column format. Manuscripts must be paginated and double-spaced throughout. Use Symbol font for all Greek characters. Do not import the figures into the text file but indicate their approximate locations directly on the manuscript. The manuscript file should be smaller than 5 MB in size.

Title page. The title page must include 1) the title of the paper, 2) name(s) and affiliation(s) of the author(s), 3) a statement indicating to whom correspondence and proofs should be sent along with a complete mailing address, telephone/fax numbers, and e-mail address, and 4) up to five key words or phrases.

Abstract. A one-paragraph abstract consisting of no more than 250 words must be included. It should state the purpose of the study, basic procedures used, main findings, and conclusions.

Abbreviations. All nonstandard abbreviations must be listed in alphabetical order, giving each abbreviation followed by its spelled-out version. Spell out the term upon first mention and follow it with the abbreviated form in parentheses. Thereafter, use the abbreviated form.

Introduction. The introduction should be a concise statement of the basis for the study and its scientific context.

Materials and Methods. Subsections under this heading should include sufficient instruction to replicate experiments, but well-established protocols may be simply referenced. *Drug Discoveries & Therapeutics* endorses the principles of the Declaration of Helsinki and expects that all research involving humans will have been conducted in accordance with these principles. All laboratory animal studies must be approved by the authors' Institutional Review Board(s).

Results. The results section should provide details of all of the experiments that are required to support the conclusions of the paper. If necessary, subheadings may be used for an orderly presentation. All figures, tables, and photographs must be referred in the text.

Discussion. The discussion should include conclusions derived from the study and supported by the data. Consideration should be given to the impact that these conclusions have on the body of knowledge in which context the experiments were conducted. In Brief Reports, Results and Discussion sections must be combined.

Acknowledgments. All funding sources should be credited in the Acknowledgments section. In addition, people who contributed to the work but who do not fit the criteria for authors should be listed along with their contributions.

References. References should be numbered in the order in which they appear in the text. Cite references in text using a number in parentheses. Citing of unpublished results and personal communications in the reference list is not recommended but these sources may be mentioned in the text. For all references, list all authors, but if there are more than fifteen authors, list the first three authors and add "et al." Abbreviate journal names as they appear in PubMed. Web references can be included in the reference list.

Example 1:

Hamamoto H, Akimitsu N, Arimitsu N, Sekimizu K. Roles of the Duffy antigen and glycoporphin A in malaria infection and erythrocyte. *Drug Discov Ther.* 2008; 2:58-63.

Example 2:

Zhao X, Jing ZP, Xiong J, Jiang SJ. Suppression of experimental abdominal aortic aneurysm by tetracycline: a preliminary study. *Chin J Gen Surg.* 2002; 17:663-665. (in Chinese)

Example 3:

Mizuochi T. Microscale sequencing of N-linked oligosaccharides of glycoproteins using hydrazinolysis, Bio-Gel P-4, and sequential exoglycosidase digestion. In: *Methods in Molecular Biology: Vol. 14 Glycoprotein analysis in biomedicine* (Hounsell T, ed.). Humana Press, Totowa, NJ, USA, 1993; pp. 55-68.

Example 4:

Drug Discoveries & Therapeutics. Hot topics & news: China-Japan Medical Workshop on Drug Discoveries and Therapeutics 2007. <http://www.ddtjournal.com/hotnews.php> (accessed July 1, 2007).

Figure legends. Include a short title and a short explanation. Methods described in detail in the Materials and methods section should not be repeated in the legend. Symbols used in the figure must be explained. The number of data points represented in a graph must be indicated.

Tables. All tables should have a concise title and be typed double-spaced on pages separate from the text. Do not use vertical rules. Tables should be numbered with Roman numerals consecutively in accordance with their appearance in the text. Place footnotes to tables below the table body and indicate them with lowercase superscript letters.

Language editing. Manuscripts submitted by authors whose primary language is not English should have their work proofread by a native English speaker before submission. The Editing Support Organization can provide English proofreading, Japanese-English translation, and Chinese-English translation services to authors who want to publish in *Drug Discoveries & Therapeutics* and need assistance before submitting an article. Authors can contact this organization directly at <http://www.iacmhr.com/iac-eso>.

IAC-ESO was established in order to facilitate manuscript preparation by researchers whose native language is not English and to help edit work intended for international academic journals. Quality revision, translation, and editing services are offered by our staff, who are native speakers of particular languages and who are familiar with academic writing and journal editing in English.

4. Figure Preparation

All figures should be clear and cited in numerical order in the text. Figures must fit a one- or two-column format on the journal page: 8.3 cm (3.3 in.) wide for a single column; 17.3 cm (6.8 in.) wide for a double column; maximum height: 24.0 cm (9.5 in.). Only use the following fonts in the figure: Arial and Helvetica. Provide all figures as separate files. Acceptable file formats are JPEG and TIFF. Please note that files saved in JPEG or TIFF format in PowerPoint lack sufficient resolution for publication. Each Figure file should be smaller than 10 MB in size. Do not compress files. A fee is charged for a color illustration or photograph.

5. Online Submission

Manuscripts should be submitted to *Drug Discoveries & Therapeutics* online at <http://www.ddtjournal.com>. The manuscript file should be smaller than 10 MB in size. If for any reason you are unable to submit a file online, please contact the Editorial Office by e-mail: office@ddtjournal.com.

Editorial and Head Office

Wei TANG, MD PhD
Secretary-in-General
TSUIN-IKIZAKA 410,
2-17-5 Hongo, Bunkyo-ku,
Tokyo 113-0033,
Japan
Tel: 03-5840-9697
Fax: 03-5840-9698
E-mail: office@ddtjournal.com

Cover letter. A cover letter from the corresponding author including the following information must accompany the submission: name, address, phone and fax numbers, and e-mail address of the corresponding author. This should include a statement affirming that all authors concur with the

submission and that the material submitted for publication has not been previously published and is not under consideration for publication elsewhere and a statement regarding conflicting financial interests.

Authors may recommend up to three qualified reviewers other than members of Editorial board. Authors may also request that certain (but not more than three) reviewers not be chosen.

The cover letter should be submitted as a Microsoft Word (.doc) file (smaller than 1 MB) at the same time the work is submitted online.

6. Accepted Manuscripts

Proofs. Rough galley proofs in PDF format are supplied to the corresponding author via e-mail. Corrections must be returned within 4 working days of receipt of the proofs. Subsequent corrections will not be possible, so please ensure all desired corrections are indicated. Note that we may proceed with publication of the article if no response is received.

Transfer of copyrights. Upon acceptance of an article, authors will be asked to agree to a transfer of copyright. This transfer will ensure the widest possible dissemination of information. A letter will be sent to the corresponding author confirming receipt of the manuscript. A form facilitating transfer of copyright will be provided. If excerpts from other copyrighted works are included, the author(s) must obtain written permission from the copyright owners and credit the source(s) in the article.

Cover submissions. Authors whose manuscripts are accepted for publication in *Drug Discoveries & Therapeutics* may submit cover images. Color submission is welcome. A brief cover legend should be submitted with the image.

Revised February 2009



Drug Discoveries & Therapeutics



Editorial Office

TSUIN-IKIZAKA 410,
2-17-5 Hongo, Bunkyo-ku,
Tokyo 113-0033, Japan

Tel: 03-5840-9697

Fax: 03-5840-9698

E-mail: office@ddtjournal.com

URL: www.ddtjournal.com

JOURNAL PUBLISHING AGREEMENT

Ms No:

Article entitled:

Corresponding author:

To be published in Drug Discoveries & Therapeutics

Assignment of publishing rights:

I hereby assign to International Advancement Center for Medicine & Health Research Co., Ltd. (IACMHR Co., Ltd.) publishing Drug Discoveries & Therapeutics the copyright in the manuscript identified above and any supplemental tables and illustrations (the articles) in all forms and media, throughout the world, in all languages, for the full term of copyright, effective when and if the article is accepted for publication. This transfer includes the rights to provide the article in electronic and online forms and systems.

I understand that I retain or am hereby granted (without the need to obtain further permission) rights to use certain versions of the article for certain scholarly purpose and that no rights in patent, trademarks or other intellectual property rights are transferred to the journal. Rights to use the articles for personal use, internal institutional use and scholarly posting are retained.

Author warranties:

I affirm the author warranties noted below.

- 1) The article I have submitted to the journal is original and has not been published elsewhere.
- 2) The article is not currently being considered for publication by any other journal. If accepted, it will not be submitted elsewhere.
- 3) The article contains no libelous or other unlawful statements and does not contain any materials that invade individual privacy or proprietary rights or any statutory copyright.
- 4) I have obtained written permission from copyright owners for any excerpts from copyrighted works that are included and have credited the sources in my article.
- 5) I confirm that all commercial affiliations, stock or equity interests, or patent-licensing arrangements that could be considered to pose a financial conflict of interest regarding the article have been disclosed.
- 6) If the article was prepared jointly with other authors, I have informed the co-authors(s) of the terms of this publishing agreement and that I am signing on their behalf as their agents.

Your Status:

I am the sole author of the manuscript.

I am one author signing on behalf of all co-authors of the manuscript.

Please tick one of the above boxes (as appropriate) and then sign and date the document in black ink.

Signature:

Date:

Name printed:

Please return the completed and signed original of this form by express mail or fax, or by e-mailing a scanned copy of the signed original to:

Drug Discoveries & Therapeutics office
TSUIN-IKIZAKA 410, 2-17-5 Hongo,
Bunkyo-ku, Tokyo 113-0033, Japan
e-mail: proof-editing@ddtjournal.com
Fax: +81-3-5840-9698

